Adequacy of Lyapunov Control of Power Systems Considering Modelling Details and Control Indices

Abdul Saleem Mir, Abhinav Kumar Singh, Bikash C. Pal, Nilanjan Senroy and Junjie Tu

***Abstract*— Nonlinear excitation controllers for power systems are considered as promising replacements for their linear counterparts, such as power system stabilizers (PSSs). However, Lyapunov based nonlinear controllers currently available in literature have been derived using simplified third order machine dynamics and have not been tested on realistic power system models, and the costs associated with these controllers have also not been studied. The paper aims to assess the performance of existing Lyapunov controllers for a detailed benchmark power system model. Two new Lyapunov based nonlinear controllers have been derived using IEEE recommended subtransient machine model, and their performance and costs have been compared with existing methods. The controllers have been evaluated using metrics for both small signal stability and transient stability. It has been proven theoretically (via stability analysis) and demonstrated via simulations that proposed Lyapunov controllers are more viable options for control of power system oscillatory dynamics. It has also been demonstrated that detailed subtransient model is required for accurate estimation of states via dynamic state estimation for use in the realization of Lyapunov controllers.**

***Index Terms*— Nonlinear controller, power system dynamics, small signal stability, modal analysis, normal-form, Lyapunov, transient stability, critical clearing time, voltage regulation.**

NOMENCLATURE

p	Machine index.
i, j	General subscript for the i^{th} or j^{th}
ω_s, ω	Synchronous and Mach. rotor speeds in rad./s resp.
P_{e}, I	Electrical power and stator current in *p.u.* resp.
δ, θ	Rotor angle and stator voltage phase angle in *rad.*
V_a, E_{fd}	AVR regulator voltage, field excitation voltage
V_r, V_{ss}	AVR filter voltage and PSS/controller output resp.
E'_d, E'_q	Transient *d* and *q* axis emfs in *p.u.*
ψ_d, ψ_q	Subtransient damper coil *d* and *q* axis emfs in *p.u.*
V_q, V_d	*q* and *d* axis stator voltages in *p.u.*
$V_{\mathrm{Q}}, V_{\mathrm{D}}$	*q* and *d* axis stator voltages in *p.u.*, in network frame of reference
I_q, I_d	*q* and *d* axis stator currents in *p.u.*
$I_{\mathrm{Q}}, I_{\mathrm{D}}$	*q* and *d* axis generator currents in *p.u.* in network frame of reference
E'_{dc}	transient emf across dummy rotor coil, in p.u.
D	Damping constant (*p.u.*)
H	Inertia constant, in seconds, $\mathrm{M} = 2\mathrm{H}$
T_m, T_e	Mechanical and electrical torque, in *p.u.* resp.
P_m, P_e	Mechanical and electrical power, in *p.u.* resp.
T'_{d0}	d-axis open circuit sub-transient time constant (s).
T'_{q0}	q-axis open circuit sub-transient time constant (s).
T_c	dummy rotor coil time constant (s).
x_d	d-axis synchronous reactance, in p.u.
x'_d	d-axis transient reactance, in p.u.
x''_d	d-axis subtransient reactance, in p.u.
x_q	q-axis synchronous reactance, in p.u.
x'_q	q-axis transient reactance, in p.u.
x''_q	q-axis subtransient reactance, in p.u.
x_l	Armature leakage reactance, in p.u.
K_{d1}	Defined as $(x''_d - x_l)/(x'_d - x_l)$
K_{d2}	Defined as $(x''_d - x'_d)/(x'_d - x_l)$
K_{q1}	Defined as $(x''_q - x_l)/(x'_q - x_l)$
K_{q2}	Defined as $(x''_q - x'_q)/(x'_q - x_l)$
V_t	Generator terminal voltage, in p.u.
ps_p	Controller states (including washout filter).
$(\tilde{.})$	$(.) - (.)_0$; State variable transformation
x, μ	State and input vectors respectively
y, n_x	Measurement vector, State vector dimension.
R_a	Armature resistance, in p.u.; K_S PSS gain
K_A, n_μ	ST1A gain, Control vector dimension.
$\mathbf{V}, \mathbf{I}$	Bus voltages and bus current injection vectors resp.
N	Number of nodes in the power system network.
$T_{\mathrm{CH}}, T_{\mathrm{SV}}$	Time constants of the turbine and governor resp.
$P_{\mathrm{CH}}, P_{\mathrm{SV}}$	Steam chest power output and valve position resp.
$P_{\mathrm{C}}, R_{\mathrm{D}}$	Governor set point and regulation constant resp.
PSS	Power system stabilizer; CCT Critical clearing time
AVR	Automatic voltage regulator

I. INTRODUCTION

EXCITATION control of multi-machine power systems has been of interest to researchers and engineers as it directly decides the system stability. The design of an excitation controller has the following objectives [1]: *a*) to be optimally adapted to the system mathematical model, *b*) to be decentralized so that control decisions rely only on local measurements, *c*) to be immune to changes in system set points and operating conditions, *d*) not be affected by large disturbances, and *e*) robust to measurement sensor anomalies. Commonly used auxiliary linear controllers, such as PSSs, are not perfect solutions to these challenges. A multi-machine power system is non-linear in nature and any disturbances are likely to significantly change the operating point of the system. For linear controllers based on linear control theories, linearization of the system is required in the neighborhood of a pre-determined system equilibrium or a

This work was supported by EPSRC UK under Grant EP/T021713/1. This article has been accepted for publication in IEEE Transactions on Power Systems. For the purpose of open access, the author has applied a Creative Commons Attribution (CC BY) licence to any Author Accepted Manuscript version arising. Citation : DOI 10.1109/TPWRS.2022.3180397

Abdul Saleem Mir is with the Department of Electrical Engineering, Indian Institute of Technology Roorkee, India; (email; saleemmir@ee.iitr.ac.in), Abhinav Kumar Singh is with the School of Electronics and Computer Science, University of Southampton, UK (email: a.k.singh@soton.ac.uk). Bikash C. Pal is with the Electrical and Electronic Engineering Department, Imperial College, London U.K. (e-mail: b.pal@imperial.ac.uk), Nilanjan Senroy is with the Department of Electrical Engineering, Indian Institute of Technology Delhi, India; (email: nsenroy@ee.iitd.ac.in), and Junjie Tu was with the Electrical and Electronic Engineering Department, Imperial College, London U.K.(email:junjie.tu16@imperial.ac.uk).

set of equilibria. Such controllers are only valid in such a neighborhood and any significant change in the system may cause stability problems. Additionally, linear state feedback controllers may be sluggish as they require linearization of the system dynamics and their optimality depends on the adequacy of the system dynamic model [1]-[14]. Recently, with the systematic development of nonlinear control theory, nonlinear controllers have been proposed as a better solution.

Various nonlinear controllers proposed in power system literature may be broadly divided into two categories: methods based on normal forms [1]-[5] and methods based on Lyapunov functions [6]-[10]. Normal form-based methods involve transforming the system using a curvilinear coordinate system, while Lyapunov based methods involve finding a positive non-increasing energy-like function of the system states. Although significant development has been made in control design using both the techniques, there are still a few drawbacks of the existing methods. Firstly, most non-linear controllers are derived from a third-order model of a synchronous machine. Such model is a simplified representation of generator dynamics and cannot characterize subtransient dynamics of a machine. A controller derived from such a model may have unexpected effect on a power system and may even affect local stability at the machine [11]-[12][13]. To the best of the authors' knowledge, only one paper has shown the importance and necessity of using detailed models for deriving nonlinear controllers based on normal forms [14], while a corresponding study on Lyapunov control is not available in power system literature. The Lyapunov controllers available in literature have only been implemented and simulated on a simple network modelled using third-order machine models. This makes it unclear if these controllers are capable of being applied to realistic power systems. Also, a comparative study of existing Lyapunov controllers is not available in literature. Similarly, the performance of such controllers considering costs of control and instrumentation chain anomalies has not been studied. Finally, it is assumed that states required for realization of these controllers [1]-[10] are directly available as measurements which may be a gross approximation.

This paper aims to address the aforementioned drawbacks by finding answers to the following questions:

1. Are Lyapunov controllers based on third-order machine model compatible with (or work with) a realistic network model with detailed machine models?
2. How do different nonlinear controllers perform compared to each other?
3. What is the impact of model order on the accurate estimation of machine states for use in the realization of these controllers?
4. Does the performance of Lyapunov control improve if controllers are derived from sixth-order model?
5. Are the controllers (derived from third or sixth-order machine model) realizable in practice considering costs of control and instrumentation chain anomalies? And is computation an issue in realizing these Lyapunov controllers derived from third or sixth order models?

In this paper, two representative Lyapunov controllers have been tested using the 68-bus benchmark power system [15]. The proposed controllers are based on the subtransient machine dynamics and focus on both small signal and transient stability. Specifically, the following metrics have been evaluated and compared for all the tested controllers: modal analysis, an index for transient stability (integrated variation of per-unit rotor energy), critical clearing time (CCT), control cost and voltage regulation. The principle contributions/advantages of this work are as follows:

1. Two new decentralized nonlinear excitation controllers based on detailed IEEE 2.2 model have been proposed for control of oscillatory dynamics and overall stability improvement. One controller is based on feedback linearization (namely LYPF1) while the second (namely LYPF2) is based on nonlinear optimal control. Compared to all other Lyapunov controllers LYPF2 uses reduced control effort while increasing the stability margins. Additionally, it does not contain any derivative term in the control law unlike other Lyapunov controllers.
2. The compatibility, performance, and control efforts of the Lyapunov controllers based on simplistic and detailed machine models has been thoroughly studied and compared, to answer the above questions.
3. Estimated states via dynamic state estimation (DSE) have been used in realizing all the controllers to eliminate the gross approximation about the availability of machine states as direct measurements. It has also been established that DSE based on detailed machine models is necessary to accurately estimate the machine states for use in the Lyapunov controllers based on any model order.
4. The asymptotic stability of the system with the derived controllers has been proven analytically. Theoretical findings are complimented by performing eigen-value analysis of a test system with the derived controllers.
5. The feasibility of the application of the Lyapunov controllers including proposed ones (LYPF1 and LYPF2) has also been discussed by comparing their computational requirements and real-time tests.

The rest of the paper is organized as follows: Section II reviews synchronous machine models and Section III briefly introduces the controllers being studied. Section IV presents the concise derivation of the two new controllers. Section V presents the stability analysis of the proposed controllers. Section VI introduces the detailed case studies and presents the comparison results and inferences followed by conclusions in Section VII.

II. Power System Model

The dynamics of a conventional power system are dominated by generator behavior. Depending upon the application, a synchronous generator can be represented by mathematical models at different complexities with certain assumptions and modelling approximations. The model complexity of a synchronous machine is reflected by the numbers of damper coils on its rotor [16], [17]. The sixth-order model is the recommended model as per IEEE [11], with a field winding and a damper coil on d-axis and two damper coils on q-axis. It is known as sub-transient model,

or Model 2.2, described using set of equations given in Appendix-A [18]-[20].

III. Lyapunov Controllers Based on Simplistic Models

Unlike normal form-based controllers, Lyapunov function based controllers do not have a uniform derivation methodology. It varies with different choices of Lyapunov function. It is required that any Lyapunov function must be radially unbounded and positive definite while the time-derivative of the function along system trajectory is required to be negative definite.

The two Lyapunov controllers based on simplistic third-order machine model, as studied and compared in this paper, are obtained from [6]-[7], with the first controller given by:

$$E_{fdi} = C_{2i}^{-1}(-17\Delta P_{ei} + 18\Delta\omega_i - 65\Delta \mathrm{V}_{ti} - C_{1i}) \quad (1)$$

where $C_{1i} = \mathrm{V}_{ti}^{-1}[-V_{di}x'_{qi}\dot{I}_{qi} + V_{qi}(x'_{di}\dot{I}_{di} + {T'_{d0}}^{-1}E'_{qi})]$ and $T'_{d0i}C_{2i} = \mathrm{V}_{ti}^{-1}V_{qi}$. The second controller given by:

$$E_{fdi} = u_i = -a_{2i}z_{2i} - q_{3i}z_{3i} - \hat{\boldsymbol{\theta}}_i^{\,T}\boldsymbol{\xi}_i - S(\hat{\boldsymbol{\beta}}_i^{\,T}\boldsymbol{\eta}_i z_{3i})\hat{\boldsymbol{\beta}}_i^{\,T}\boldsymbol{\eta}_i \quad (2)$$

with the following definition:

$z_{1i} = x_{1i},\ z_{2i} = x_{2i} - u_{1i},\ z_{3i} = x_{3i} - u_{2i},\ u_{1i} = -q_{1i}z_{1i},\ u_{2i} = -a_{2i}^{-1}q_{2i}z_{2i} - a_{2i}^{-1}z_{1i} - a_{2i}^{-1}(a_{1i} + q_{1i})x_{2i},\quad S(x) = \rho_1 arctan(\rho_2 x)$, where 5, 5, 5, 1 and 156 are chosen respectively for q_{1i}, q_{2i}, q_{3i}, ρ_1 and ρ_2. $\hat{\boldsymbol{\theta}}_i$ and $\hat{\boldsymbol{\beta}}_i$ meets adaptive law: $\dot{\hat{\boldsymbol{\theta}}}_i = \boldsymbol{\xi}_i z_{3i}$, $\dot{\hat{\boldsymbol{\beta}}}_i = |\boldsymbol{\eta}_i z_{3i}| - \alpha_i\hat{\boldsymbol{\beta}}_i$.

The controllers (1) and (2) are referred to as LYP1 & LYP2, respectively.

Remark 1: In MATLAB implementation, use of derivative block should be avoided in Simulink as it is treated as a zero gain when linearized [21]. Instead, it can be replaced by an approximate lead compensator transfer function $Ns/(Ns + 1)$ (N is a large positive number).

IV. Lyapunov Controllers Based on Detailed Model

A. Feedback Linearization based Lyapunov control

Feedback linearization involves transformation of a detailed nonlinear model into a linear equivalent paradigm through a change of variables while exactly preserving the system nonlinearity in the transformed model [22]-[27]. To study the effect of machine model on control design, a Lyapunov function based controller has been derived from a sixth-order machine model. The derivation is similar to the derivation of LYP1 in [6]. For the i^{th} machine, if the deviations in generated power, rotor speed and terminal voltage from their respective nominal values are selected as output, then:

$$y_i = [\Delta P_{ei}\ \Delta\omega_i\ \Delta \mathrm{V}_{ti}]^T \quad (3)$$

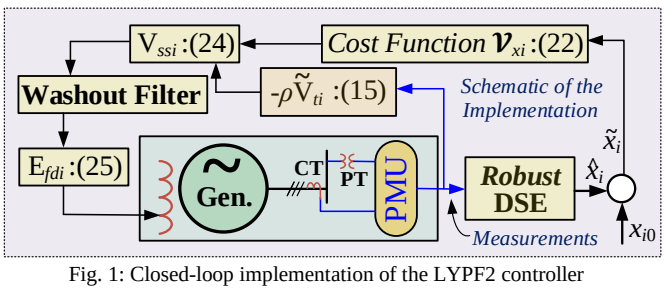

Fig. 1: Closed-loop implementation of the LYPF2 controller

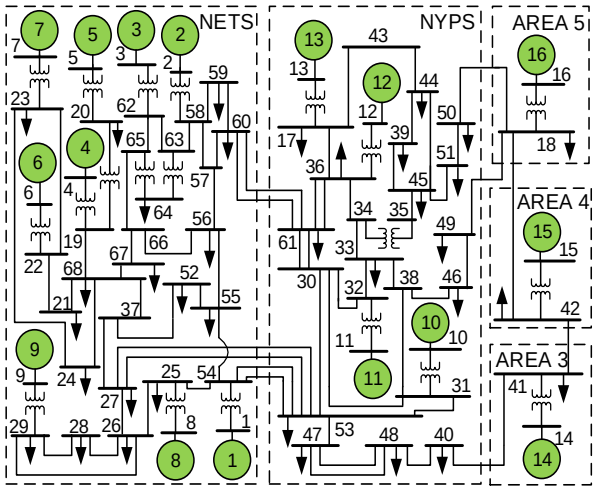

Fig. 2: Simplified line diagram of NETS-NYPS test system [14]

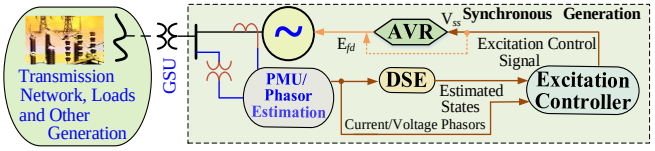

Fig. 3: Schematic of the realization of controllers.

The Lyapunov function is chosen to be:

$$\mathrm{V}_i(y_i) = 2^{-1}[\Delta P_{ei}^2 + \Delta\omega_i^2 + \Delta \mathrm{V}_{ti}^2] \quad (4)$$

As V_i is a sum of quadratic terms, it can be easily verified that it is positive definite and radially unbounded. The time-derivative of $\mathrm{V}_i(y_i)$ along the power system can be simply written as:

$$\dot{\mathrm{V}}_i(y_i) = {y_i}^T\dot{y}_i, \text{ where } \dot{y}_i = [\Delta\dot{P}_{ei}\ \Delta\dot{\omega}_i\ \Delta\dot{\mathrm{V}}_{ti}]^T \quad (5)$$

In order to achieve global asymptotic stability, the trajectory of derivative $\dot{y}_i$ is constructed as a linear control system written as [6]:

$$\dot{y}_i = A_i y_i + B_i v_i \quad (6)$$

where $A_i = \begin{bmatrix} -2 & 1 & 0 \\ 1 & -2 & 1 \\ 0 & 0 & 0 \end{bmatrix}$ and $B_i = \begin{bmatrix} 0 \\ 0 \\ 1 \end{bmatrix}$.

The virtual input v_i equals the time-derivative of terminal voltage. The next step is to calculate the time-derivative of terminal voltage V_{ti}, which satisfies (7).

$$\mathrm{V}_{ti}^2 = V_{di}^2 + V_{qi}^2 \quad (7)$$

As V_{di} and V_{qi} are algebraic functions of time, for convenience, they are denoted as $b(t)$ and $c(t)$ and V_{ti}^2 is denoted as $a(t)$. The derivative is:

$$\frac{d\mathrm{V}_{ti}}{dt} = a^{-\frac{1}{2}}(t)\frac{da(t)}{dt} = \frac{1}{2}a^{-\frac{1}{2}}\left(2b(t)\frac{db(t)}{dt} + 2c(t)\frac{dc(t)}{dt}\right)$$

Substituting (A9.1) and (A9.2) from Appendix-A to replace $b(t)$ and $c(t)$.

$$v_i = S_{1i} + S_{2i}E_{fdi} \quad (8)$$

where $S_{1i} = \mathrm{V}_{ti}^{-1}[V_{di}(K_{q1i}\dot{E}'_{di} - K_{q2i}\dot{\psi}_{2qi} - x''_{qi}\dot{I}_{qi}) + V_{qi}(K_{d2i}\dot{\psi}_{1di} + x''_{di}\dot{I}_{di} + K_{d1i}\dot{E}''_{qi}/T'_{d0})]$ and $S_{2i} = K_{d1i}V_{qi}/(\mathrm{V}_{ti}T'_{d0i})$. Finally, applying feedback, the virtual input v_i is:

$$v_i = -k_{1i}\Delta P_{ei} - k_{2i}\Delta\omega_i - k_{3i}\Delta \mathrm{V}_{ti} \quad (9)$$

By substituting the virtual input and the constructed trajectory of derivative, the expression of $\dot{\mathrm{V}}_i$ is:

$$\dot{\mathrm{V}}_i = y_i^T H_i \dot{y}_i \quad (10)$$

where $H_i = \begin{bmatrix} -2 & 1 & 0 \\ 1 & -2 & 1 \\ -k_{1i} & -k_{2i} & -k_{3i} \end{bmatrix}$.

It is required that $\dot{V}_i$ must be negative definite in order to achieve global asymptotic stability. The gains vector $[k_{1i} \quad k_{2i} \quad k_{3i}] = [17 \quad -18 \quad 65]$ (obtained via pole placement technique [24]) ensures $\dot{V}_i$ is negative definite. Hence, the final control expression is:

$$E_{fdi} = S_{2i}^{-1}(-17\Delta P_{ei} + 18\Delta\omega_i - 65\Delta V_{ti} - S_{1i}) \quad (11)$$

with S_{1i} and S_{2i} as expressed as earlier. This Controller (11) is referred to as LYPF1.

B. Nonlinear State-feedback Optimal Control

The Affine representation of the subtransient dynamics (A1)-(A10) is given by (12) after transforming the state and control variables as $\tilde{\boldsymbol{x}}_i = \boldsymbol{x_i} - \boldsymbol{x}_{0i}$ and $\tilde{\boldsymbol{\mu}}_i = \boldsymbol{\mu_i} - \boldsymbol{\mu}_{0i}$. where, $\boldsymbol{x_i} = [\Delta\delta_i \; \Delta\omega_i \; E'_{di} \; E'_{qi} \; \psi_{di} \; \psi_{qi} \; E_{dci} \; V_{ri}]^{\mathrm{T}}$ and $\boldsymbol{\mu_i} = V_{ssi}$.

$$\dot{\tilde{\boldsymbol{x}}}_i = \boldsymbol{f}(\tilde{\boldsymbol{x}}_i) + \boldsymbol{g}(\tilde{\boldsymbol{x}}_i)\tilde{\boldsymbol{\mu}}_i + \boldsymbol{l}(\tilde{\boldsymbol{x}}_i)\tilde{V}_{ti} \quad (12)$$

The voltage deviation $\tilde{V}_t$ in (34) acts as an 'exogenous input' to a nonlinear system (34).

Remark 2: An 'exogenous input' to a system is an input whose magnitude cannot be altered by design. If an exogenous input is measurable, it is possible to cancel out or minimize its effect by incorporating it in a control law.

Therefore, (12) can be rewritten as (13).

$$\dot{\tilde{\boldsymbol{x}}}_i = \boldsymbol{f}(\tilde{\boldsymbol{x}}_i) + \boldsymbol{g}(\tilde{\boldsymbol{x}}_i)\tilde{\boldsymbol{\mu}}'_i + \boldsymbol{g}(\tilde{\boldsymbol{x}}_i)\tilde{\boldsymbol{\mu}}''_i + \boldsymbol{l}(\tilde{\boldsymbol{x}}_i)\tilde{V}_{ti} \quad (13)$$

where, $\tilde{\boldsymbol{\mu}}_i = \tilde{\boldsymbol{\mu}}'_i + \tilde{\boldsymbol{\mu}}''_i$. $\tilde{\boldsymbol{\mu}}'_i$ corresponds to feedback control law whereas $\tilde{\boldsymbol{\mu}}''_i$ design incorporates $\tilde{V}_t$ in the control law to stabilize this deviation and thereby mitigates its impact on the system dynamics by minimizing $\mathbf{H_1}$ (quadratic cost function given by (14)).

$$\mathbf{H_1} = \left[\boldsymbol{g}(\tilde{\boldsymbol{x}}_i)\tilde{\boldsymbol{\mu}}''_i + \boldsymbol{l}(\tilde{\boldsymbol{x}}_i)\tilde{V}_{ti}\right]^{\mathbf{T}}\left[\boldsymbol{g}(\tilde{\boldsymbol{x}}_i)\tilde{\boldsymbol{\mu}}''_i + \boldsymbol{l}(\tilde{\boldsymbol{x}}_i)\tilde{V}_{ti}\right] \quad (14)$$

$\partial\mathbf{H_1}/\,\partial\tilde{\boldsymbol{\mu}}''_i = 0$ yields the following law for $\tilde{\boldsymbol{\mu}}''_i$.

$$\tilde{\boldsymbol{\mu}}''_i = -[\boldsymbol{g}^{\boldsymbol{T}}(\tilde{\boldsymbol{x}}_i)\boldsymbol{g}(\tilde{\boldsymbol{x}}_i)]^{-\mathbf{1}}\boldsymbol{g}^{\boldsymbol{T}}(\tilde{\boldsymbol{x}}_i)\boldsymbol{l}(\tilde{\boldsymbol{x}}_i)\tilde{V}_{ti} = -\rho\tilde{V}_{ti} \quad (15)$$

where, $\rho = [\boldsymbol{g}^{\boldsymbol{T}}(\tilde{\boldsymbol{x}}_i)\boldsymbol{g}(\tilde{\boldsymbol{x}}_i)]^{-\mathbf{1}}\boldsymbol{g}^{\boldsymbol{T}}(\tilde{\boldsymbol{x}}_i)\boldsymbol{l}(\tilde{\boldsymbol{x}}_i)$ is a scalar quantity. The design equation (15) ensures $\boldsymbol{g}(\tilde{\boldsymbol{x}}_i)\tilde{\boldsymbol{\mu}}''_i + \boldsymbol{l}(\tilde{\boldsymbol{x}}_i)\tilde{V}_{ti} \to 0$. Therefore, equation (13) assumes the following form.

$$\dot{\tilde{\boldsymbol{x}}}_i \approx \boldsymbol{f}(\tilde{\boldsymbol{x}}_i) + \boldsymbol{g}(\tilde{\boldsymbol{x}}_i)\tilde{\boldsymbol{\mu}}'_i \quad (16)$$

The optimal control *value function* (Lyapunov function candidate) [22]-[23] (17) used to derive the feedback control law $\tilde{\boldsymbol{\mu}}'_i$ for the dynamical system (16) after cancelling the effect of $\tilde{V}_{ti}$ via $\tilde{\boldsymbol{\mu}}''_i$ design is defined as

$$\mathcal{V}(\tilde{\boldsymbol{\mu}}'_i, \tilde{\boldsymbol{x}}_i) = \int_{t_0}^{\infty}\left(Q(\tilde{\boldsymbol{x}}_i) + (\tilde{\boldsymbol{\mu}}'_i)^{\mathrm{T}}R(\tilde{\boldsymbol{\mu}}'_i)\right)d\tau \quad (17)$$

where $Q(\tilde{\boldsymbol{x}}_i) > 0 \; \forall \; \tilde{\boldsymbol{x}}_i \neq \mathbf{0}$ and $\tilde{\boldsymbol{x}}_i = \mathbf{0} \Rightarrow Q(\tilde{\boldsymbol{x}}_i) = 0$, $R = R^{\mathrm{T}} > 0$ and $R \in \mathcal{R}^{n_\mu \times n_\mu}$ is a positive-definite-matrix.

Differentiating (17),

$$\Rightarrow 0 = Q(\tilde{\boldsymbol{x}}_i) + (\tilde{\boldsymbol{\mu}}'_i)^{T}R(\tilde{\boldsymbol{\mu}}'_i) + \boldsymbol{\mathcal{V}}_{\boldsymbol{xi}}^{\mathrm{T}}(\boldsymbol{f}(\tilde{\boldsymbol{x}}_i) + \boldsymbol{g}(\tilde{\boldsymbol{x}}_i)\tilde{\boldsymbol{\mu}}'_i) \equiv \mathbf{H_2} \quad (18)$$

where, $\boldsymbol{g}(\tilde{\boldsymbol{x}}_i) = [0 \; 0 \; 0 \; K_{Ai}/T'_{d0i} \; 0 \; 0 \; 0 \; 0]$, $\boldsymbol{\mathcal{V}}_{xi} = \partial\mathcal{V}/\partial\tilde{\boldsymbol{x}}_i$.

The optimal control signal $\tilde{\boldsymbol{\mu}}'_i$ is derived from (18) by using the Pontryagin's minimum principle based stationary conditions [23]. These stationary conditions are given by (19) whereas the corresponding control law derived from it is given by (20). This formulation is a nonlinear equivalent of a linear quadratic regulator (LQR).

$$\partial\mathbf{H_2}/\,\partial\tilde{\boldsymbol{\mu}}'_i = 0, \partial^2\mathbf{H_2}/\,\partial^2\tilde{\boldsymbol{\mu}}'_i = 2R > 0 \quad (19)$$

$$\Rightarrow \tilde{\boldsymbol{\mu}}'_i(\tilde{\boldsymbol{x}}_i) = -R^{-1}\boldsymbol{g}^{\mathbf{T}}(\tilde{\boldsymbol{x}}_i)\boldsymbol{\mathcal{V}}_{\boldsymbol{xi}}/2 \quad (20)$$

Substituting (20) in (18),

$$Q(\tilde{\boldsymbol{x}}_i) - \frac{1}{4}\boldsymbol{\mathcal{V}}_{\boldsymbol{xi}}{}^{\mathrm{T}}\boldsymbol{g}(\tilde{\boldsymbol{x}}_i)R\boldsymbol{g}^{\mathbf{T}}(\tilde{\boldsymbol{x}}_i)\boldsymbol{\mathcal{V}}_{\boldsymbol{xi}} + \boldsymbol{\mathcal{V}}_{\boldsymbol{xi}}^{\mathrm{T}}\boldsymbol{f}(\tilde{\boldsymbol{x}}_i) = 0 \quad (21)$$

Solution of (21) yields $\boldsymbol{\mathcal{V}}_{xi}$ for use in (20). Since (21) is a nonlinear algebraic equation, the value of variable $\boldsymbol{\mathcal{V}}_{xi}$ is obtained by a weight adaptive function approximation [23].

$$\therefore \; \boldsymbol{\mathcal{V}}_{xi} = \gamma^{\mathrm{T}}\partial\left(M(\tilde{\boldsymbol{x}}_i)\right)/\partial\tilde{\boldsymbol{x}}_i \quad (22)$$

where, $M(\tilde{\boldsymbol{x}}_i)=[m_{11} \; m_{12} \ldots m_{1n_x} \; m_{22} \ldots m_{2n_x} \ldots m_{n_x n_x}]$, $m_{ij} = a_i a_j$, $i \leq j$, $i, j \in [1 \; 2 \ldots n_x]$, a_i is the i^{th} element of the state vector $\tilde{\boldsymbol{x}}_i$ and γ is the tunable gain vector (Appendix-B) [23].

The controller effectiveness gets enhanced by including the terminal voltage deviation in the feedback law (15), (23) as an exogenous/pseudo control input (unlike [25]-[26], wherein voltage and frequency are used) and it enhances the system dynamic performance. Therefore,

$$\therefore \tilde{\boldsymbol{\mu}}_i(\tilde{\boldsymbol{x}}_i) = \tilde{\boldsymbol{\mu}}'_i + \tilde{\boldsymbol{\mu}}''_i = -R^{-1}\boldsymbol{g}^{\mathbf{T}}(\tilde{\boldsymbol{x}}_i)\boldsymbol{\mathcal{V}}_{\boldsymbol{xi}}/2 - \rho\tilde{V}_{ti} \quad (23)$$

$$V_{ssi} = -R^{-1}\boldsymbol{g}^{\mathbf{T}}(\tilde{\boldsymbol{x}}_i)\boldsymbol{\mathcal{V}}_{\boldsymbol{xi}}/2 - \rho\tilde{V}_{ti} \quad (24)$$

$$E_{fdi} = K_{Ai}\left(V_{refi} + V_{ssi} - V_{ri}\right) \quad (25)$$

V_{ssi} is nonzero only during dynamic conditions. The DC component in V_{ssi} is filtered out by a washout filter [15]. The controller of (25) is referred to as LYPF2 (Fig. 1).

V. System Stability with Proposed Controller

The proof of asymptotic stability for the LYPF1 follows similar procedure as given in Section-IV of [14], and is omitted here. In the case of LYPF2 controller the following lemma is defined.

Lemma 1 ([27], p. 151-152)**:** Let $\mathcal{s} = 0$ be an equilibrium of the system dynamics $\dot{\mathcal{s}} = \mathbb{G}(\mathcal{s})$ and $\Omega \in \mathcal{R}^{n_\mathcal{s}}$ be its domain. If there exists a function $N(\mathcal{s}) \in B(\Omega)$ such that

$$M_1(\mathcal{s}) \leq N(\mathcal{s}) \leq M_2(\mathcal{s}), \text{ and } N_{\mathcal{s}}^{\mathrm{T}}(\mathcal{s})\mathbb{G}(\mathcal{s}) \leq -M_3(\mathcal{s})$$

$\forall \; \mathcal{s} \in \Omega$, where $M_l(\mathcal{s})$ (l=1, 2, 3) are positive-definite-functions (PDFs) and $N_{\mathcal{s}} = \partial N(\mathcal{s})/\partial\mathcal{s}$, then the system is asymptotically stable at $\mathcal{s} = 0$.

Theorem 1: The control law (45) guarantees the asymptotic stability of the decentralized dynamics (34) and thereby guarantees the asymptotic stability of the overall power system irrespective of the operating point.

Proof: Since $\mathcal{V}(\tilde{\boldsymbol{\mu}}'_i, \tilde{\boldsymbol{x}}_i) > 0 \; \forall \; \tilde{\boldsymbol{x}}_i \neq \mathbf{0}$ and $\mathcal{V}(\tilde{\boldsymbol{\mu}}'_i, \tilde{\boldsymbol{x}}_i) = 0 \Leftrightarrow \tilde{\boldsymbol{x}}_i = \mathbf{0} \Rightarrow \mathcal{V}(\tilde{\boldsymbol{\mu}}'_i, \tilde{\boldsymbol{x}}_i)$ is a positive-definite-function defined on Ω. k-functions ([27], Lemma 4.3) $\mathcal{k}_1(.)$ and $\mathcal{k}_2(.)$ are defined on Ω.

$$\mathcal{k}_1(\|\tilde{\boldsymbol{x}}_i\|) \leq \mathcal{V}(\tilde{\boldsymbol{\mu}}'_i, \tilde{\boldsymbol{x}}_i) \leq \mathcal{k}_2(\|\tilde{\boldsymbol{x}}_i\|) \quad (26)$$

These k-functions are PDFs and therefore,

$$M_1(\tilde{\boldsymbol{x}}_i) = \mathcal{k}_1(\|\tilde{\boldsymbol{x}}_i\|) \text{ and } M_2(\tilde{\boldsymbol{x}}_i) = \mathcal{k}_2(\|\tilde{\boldsymbol{x}}_i\|)$$

The *time-derivative* of the Lyapunov function $\mathcal{V}(\tilde{\boldsymbol{\mu}}'_i, \tilde{\boldsymbol{x}}_i)$ along the decentralized system trajectory (12) is

$$\dot{\mathcal{V}}(\tilde{\boldsymbol{\mu}}'_i, \tilde{\boldsymbol{x}}_i) = \boldsymbol{\mathcal{V}}_{xi}^{\mathrm{T}}\left(\boldsymbol{f}(\tilde{\boldsymbol{x}}_i) + \boldsymbol{g}(\tilde{\boldsymbol{x}}_i)\tilde{\boldsymbol{\mu}}_i + \boldsymbol{l}(\tilde{\boldsymbol{x}}_i)\tilde{V}_{ti}\right) \quad (27)$$

Using (15), (18) equation (27) becomes.

$$\therefore \dot{\mathcal{V}}(\tilde{\boldsymbol{\mu}}'_i, \tilde{\boldsymbol{x}}_i) \leq Q(\tilde{\boldsymbol{x}}_i) + (\tilde{\boldsymbol{\mu}}'_i)^{T}R(\tilde{\boldsymbol{\mu}}'_i) = -M_3(\tilde{\boldsymbol{x}}_i) \quad (28)$$

Using Lemma 1 and combining (26) and (28), it is deduced that $\tilde{\boldsymbol{\mu}}_i$ given by (23) ensures asymptotic stability of the dynamical system (12) with pseudo-inputs $\tilde{V}_{ti}$.

The affine representation of the system dynamics of all machines of the power system may be combined using (12). Therefore,

$$\begin{bmatrix}\dot{\tilde{x}}_1\\ \dot{\tilde{x}}_2\\ \cdots\\ \dot{\tilde{x}}_p\end{bmatrix}=\begin{bmatrix}f(\tilde{x}_1)\\ f(\tilde{x}_2)\\ \cdots\\ f(\tilde{x}_p)\end{bmatrix}+\begin{bmatrix}g(\tilde{x}_1) & 0 & 0 & 0\\ 0 & g(\tilde{x}_2) & 0 & 0\\ 0 & 0 & \ddots & 0\\ 0 & 0 & 0 & g(\tilde{x}_p)\end{bmatrix}\begin{bmatrix}\tilde{\mu}_1\\ \tilde{\mu}_2\\ \cdots\\ \tilde{\mu}_p\end{bmatrix}+\begin{bmatrix}l(\tilde{x}_1) & 0 & 0 & 0\\ 0 & l(\tilde{x}_2) & 0 & 0\\ 0 & 0 & \ddots & 0\\ 0 & 0 & 0 & l(\tilde{x}_p)\end{bmatrix}\begin{bmatrix}\tilde{V}_{t1}\\ \tilde{V}_{t2}\\ \cdots\\ \tilde{V}_{tp}\end{bmatrix} \quad (29)$$

In compact form the above equation (29) can be represented as follows.

$$\dot{\mathbf{X}}_s=\mathbf{F_s}(\mathbf{X_s})+\mathbf{G_s}(\mathbf{X_s})\mathbf{U_s}+\mathbf{L_s}\mathbf{V_s} \quad (30)$$

Where,

$$\mathbf{X_s}=\begin{bmatrix}\dot{\tilde{x}}_1\\ \dot{\tilde{x}}_2\\ \cdots\\ \dot{\tilde{x}}_p\end{bmatrix},\ \mathbf{U_s}=\begin{bmatrix}\tilde{\mu}_1\\ \tilde{\mu}_2\\ \cdots\\ \tilde{\mu}_p\end{bmatrix},\ \mathbf{G_s}=\begin{bmatrix}g(\tilde{x}_1) & 0 & 0 & 0\\ 0 & g(\tilde{x}_2) & 0 & 0\\ 0 & 0 & \ddots & 0\\ 0 & 0 & 0 & g(\tilde{x}_p)\end{bmatrix},$$

$$\mathbf{L_s}=\begin{bmatrix}l(\tilde{x}_1) & 0 & 0 & 0\\ 0 & l(\tilde{x}_2) & 0 & 0\\ 0 & 0 & \ddots & 0\\ 0 & 0 & 0 & l(\tilde{x}_p)\end{bmatrix}\text{ and }\mathbf{V_s}=\begin{bmatrix}\tilde{V}_{t1}\\ \tilde{V}_{t2}\\ \cdots\\ \tilde{V}_{tp}\end{bmatrix}$$

The composite representation of the overall system dynamics (30) resembles (12). Therefore, the asymptotic stability of the system (30) is proved with **Theorem 1** while using the same sequential steps as used for the decentralized dynamics (12). It is further validated by performing the eigenvalue analysis of the overall system (detailed in Section VI.)

VI. Case Study

A. System Description and Controller Realization

The proposed controllers were tested on a 16-machine, 68 bus IEEE benchmark test system, as shown in Fig. 2. In the study, it is assumed that all machines have the controllers enabled as shown in Fig. 3. Low frequency oscillations in power systems are global as they involve generators, loads, and substantial portion of the power network. Each synchronous machine contributes to these low frequency oscillations in varying degrees [15]. Therefore, each machine is equipped with a controller to dampen out these oscillations [28], [29]. All these controllers need the interior machines states as inputs to derive the control effort. These states are estimated locally from terminal bus phasor measurements using a dynamic state estimator (DSE) [27]-[31] as shown by the schematic in Fig. 3. [15] presents a study in small signal stability when the system is controlled by PSS-AVR (see Appendix-B for PSS equations). MATLAB-Simulink platform has been used for power system modelling, controller designs and simulations.

B. Dynamic State Estimation and Model Order

Implementation/realization of control laws (1), (2), (11) and (25) requires accurate estimation of machine states as they are not measurable directly. Generator bus PMU measurements serve as inputs for the dynamic state estimator (Fig. 3). The procedure to estimate the synchronous machine states from generator bus PMU measurements uses a decentralized methodology [31]. In the DSE methodology, generator bus voltage phasor (both angle and magnitude) are used as pseudo-inputs to make the estimation process decentralized. The unscented Kalman filter based DSE is used to derive the estimates of the states dynamically [31]-[32]. If a simplistic model (A1)-(A2), (A11)-(A14) of the synchronous machine is used in the DSE, the estimated states do not follow the actual trajectory of these states due to model inadequacy whereas if the detailed subtransient model (A1)-(A10) is used in the DSE, the estimated states track the actual time trajectory of the machine states. For illustration, the dynamic estimate of the machine speed of the 13th generation unit of the test system (Fig. 2) considering simplistic and detailed order models is shown in Fig. 4. In this case study, a fault was simulated at bus 54 of the test system at $t = 1s$ and cleared by opening circuit breakers on line 53-54 at $t = 1.18s$.

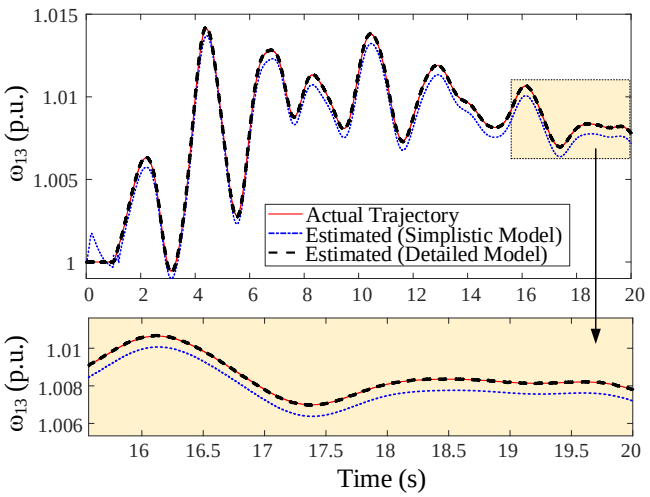

Fig. 4: Dynamic state estimation; simplistic model versus detailed model

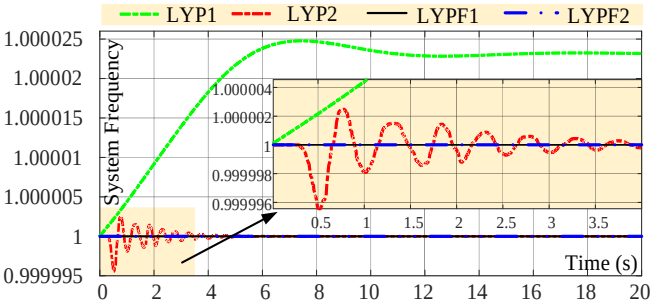

Fig. 5: Frequency transition; Base case scenario.

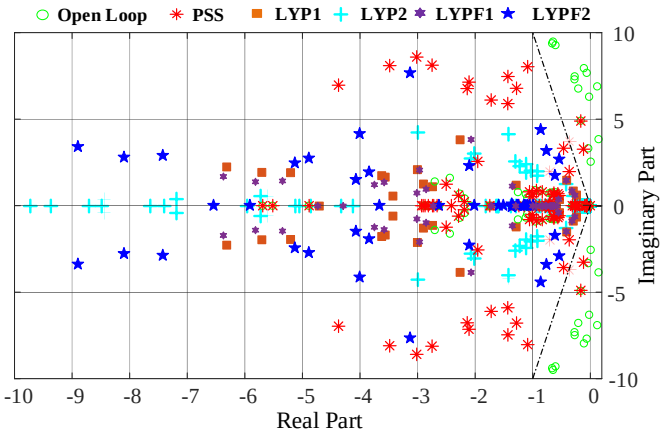

Fig. 6-Eigenvalue plot with/without Lyapunov based controllers/PSS

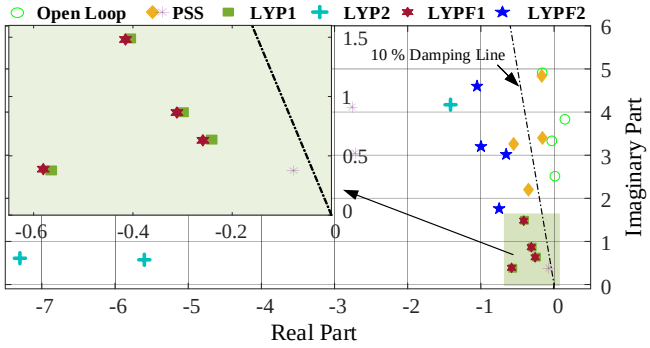

Fig. 7-Eigenvalue plot of inter-area modes with/without Lyapunov based controllers/PSS.

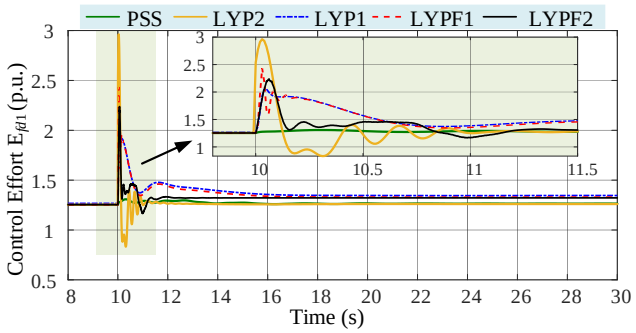

Fig. 8: Controller effort in p.u. following a step change in T_{mi} (machine 1).

C. Base Case and Lyapunov Control

The base case refers to the case of the power system at equilibrium with no external disturbance applied. It is a basic test of compatibility and demonstrates the influence of difference in model complexity. The system is expected to have a new equilibrium if controllers derived using third-order machine model are applied.

Fig. 5. shows the graphs of system frequency in time domain when the system is controlled by LYP1, LYP2, LYPF1 and LYPF2. In the case of LYP1 and LYP2 there is a transition to a new steady state value. Such transitions in frequencies occur because of mismatch in assumptions of system model and thus in assumed system equilibrium. Taking E_{fd} as an example, since the power system is modelled with sixth-order machine models, subtransient machine dynamics define the dynamics of the system. Therefore, at equilibrium, the initial excitation voltage E_{fd} for subtransient model is $E_{fd0i} = \left| E_{q0i} \right| - (x_{di} - x_{qi}) I_{d0i}$. However, the two controllers (LYP1 and LYP2) are derived from third order machine model. At the start of simulation, all quantities are at nominal values. Under such condition, excitation voltage is $E_{fd} = \left| E_q \right|$. Because of this mismatch, a transition in equilibrium values takes place. Based on this observation, any comparison should also be conducted between post-disturbance values and values at new operating point as new nominal values. For LYPF1 and LYPF2, the system remains at pre-calculated equilibrium as expected since there is no mismatch in model complexity.

D. Modal Analysis

Power system oscillations contain multiple frequency components (modes). Each eigenvalue corresponds to a mode. Modes where electromechanical states (i.e. rotor speed and rotor angle) have high participation are electromechanical modes. Among them, poorly damped low frequency oscillations ($0.2 \sim 2Hz$) (particularly inter-area oscillations [18], [33]) pose a serious threat for secure and stable operation of an interconnected power systems. Unless well damped, such oscillations hamper the transfer of large amounts of power through transmission lines [11]-[12]. With their low frequency, it takes a long time for them to settle down and thus at least 10% damping ratio [15] is desired. The eigen-value plot of the system with and without Lyapunov controllers and PSS is shown in Fig. 6. All the Lyapunov controllers improve the damping ratios of all low frequency modes including inter-area modes. TABLE I lists the damping ratios and frequencies of inter-area modes if the system is controlled by PSS, LYP1, LYP2, LYPF1 and LYPF2. The corresponding eigenvalue plot of inter-area modes for illustration is shown in Fig. 7.

TABLE I- FREQUENCY AND DAMPING RATIOS OF INTER-AREA MODES

Controller	Mode 1		Mode 2		Mode 3		Mode 4	
	$\zeta(\%)$	$f(Hz)$	$\zeta(\%)$	$f(Hz)$	$\zeta(\%)$	$f(Hz)$	$\zeta(\%)$	$f(Hz)$
Open Loop	-0.44	0.40	0.94	0.53	-3.86	0.61	3.32	0.78
PSS	15.72	0.35	14.78	0.52	4.69	0.54	3.50	0.77
LYP1	83.17	0.06	35.35	0.10	32.59	0.14	26.26	0.24
LYP2	99.48	0.09	99.90	0.10	32.13	0.66	/	/
LYPF1	83.17	0.06	37.66	0.10	33.53	0.14	27.60	0.24
LYPF2	36.01	0.31	20.21	0.49	24.58	0.52	19.63	0.73

TABLE II- NORMALIZED PARTICIPATION FACTORS

	PSS		LYP1		LYP2		LYPF1		LYPF2	
	State	NPF	State	NPF	State	NPF	State	NPF	State	NPF
Mode 1	ω_{15}	1	δ_{15}	1	ps_{14}	1	δ_{15}	1	ω_{15}	1
	ω_{16}	0.83	ω_{15}	0.93	δ_{14}	0.61	ω_{15}	0.93	δ_1	0.97
	δ_{13}	0.77	ω_{14}	0.38	$E'_{q_{14}}$	0.51	ω_{14}	0.37	δ_{15}	0.90
	ω_{16}	0.62	δ_{14}	0.32	ps_{15}	0.47	δ_{14}	0.31	ω_{13}	0.33
	δ_5	0.55	$E'_{d_{15}}$	0.10	δ_{15}	0.42	$E'_{d_{15}}$	0.08	δ_{14}	0.30
Mode 2	ω_{13}	1	δ_{14}	1	$\dot{\omega}_{16}$	1	δ_{14}	1	ω_{14}	1
	δ_{13}	0.96	ω_{14}	0.72	$E'_{q_{16}}$	0.75	ω_{14}	0.69	ω_{16}	0.98
	δ_{12}	0.62	ω_{16}	0.46	ω_{16}	0.74	ω_{16}	0.47	δ_{16}	0.87
	δ_{14}	0.30	δ_{15}	032	$\dot{\omega}_{14}$	0.68	δ_{15}	031	ω_{15}	0.51
	ω_{16}	0.30	ω_{15}	0.17	ω_{14}	0.57	ω_{15}	0.15	δ_{14}	0.30
Mode 3	δ_{14}	1	δ_{13}	1	$\dot{\omega}_{15}$	1	δ_{13}	1	δ_{13}	1
	ω_{16}	0.83	ω_{13}	0.58	ω_{15}	0.80	ω_{13}	0.58	ω_{13}	0.91
	ω_{14}	0.49	ω_{16}	0.29	δ_{15}	0.79	ω_{16}	0.26	ω_{16}	0.76
	δ_{13}	0.46	ω_{15}	0.07	δ_{15}	0.64	ω_{15}	0.09	δ_{16}	0.10
	ω_{13}	0.21	ω_{14}	0.07	$\dot{\omega}_{14}$	0.43	ω_{14}	0.08	ω_{14}	0.10
Mode 4	δ_{15}	1	ω_{13}	1	-	-	ω_{13}	1	δ_{15}	1
	ω_{15}	0.74	ω_{16}	0.50	-	-	ω_{16}	0.56	ω_{15}	0.89
	ω_{14}	0.30	δ_5	0.35	-	-	δ_5	0.35	ω_{14}	0.82
	δ_{14}	0.14	δ_6	0.29	-	-	δ_6	0.29	δ_9	0.20
	ω_{16}	0.13	δ_9	0.28	-	-	δ_9	0.26	ω_{16}	0.16

TABLE III- CONTROL EFFORT AND STATE DEVIATION

Controller	Control effort	State deviation	Total cost
PSS+AVR	14.44	54.54	68.98
LYPF2+AVR	59.61	57.74	117.35
LYP1	188.4	1114	1302.4
LYP2	3×10^4	1.358	3×10^4
LYPF1	178.3	992.2	1170.5

As shown in TABLE I and Fig. 6-Fig. 7, all controllers can handle the instability (negative damping ratio) in open loop system. However, every nonlinear controller exhibits a much higher damping ratio but a relatively lower modal frequency with respect to inter-area modes. A brief explanation of why this happens is as follows.

The studied nonlinear controllers work by changing the excitation of the rotor field windings and thereby modulate the developed electrical torque. These nonlinear controllers modulate the field winding excitation and therefore the synchronous torque produced due to interaction of stator and rotor magnetic fields. In response to a change in the dynamic states of the machine due to a disturbance, the nonlinear controllers respond immediately, and provide fast damping to any electromechanical mode of the system. The modal damping ratio increases, while modal frequency decreases significantly. Modal damping ratios in the case of LYPF2 are lower than other nonlinear controllers but much higher than PSS whereas inter-area mode frequencies remain almost same as PSS i.e., LYPF2 improves the damping of these inter-area eigenvalues significantly whereas there is minimal change in corresponding modal frequencies (Fig. 6-Fig. 7), unlike the other three nonlinear controllers.

Furthermore, a participation factor analysis [17]-[18] was also conducted to measure the sensitivity of a mode to a state. In nonlinear systems, the generic second-order expression for modes-in-states participation is given by (31) [12].

$$x_i(t) = p_{2ik} e^{\lambda_k t} + \sum_{j=1}^{n} \sum_{l=j}^{n} p_{2jl}^{i} e^{(\lambda_j + \lambda_l)t} \quad (31)$$

where, p_{2ik} represents the participation of k^{th} mode in i^{th} state and p_{2jl}^{i} represents the participation of combination of j^{th} and l^{th} modes in i^{th} state. Assuming the system is not extremely stressed and the individual components of the initial vector $x_{0i} = x_i(0)$ values are statistically independent, then the contribution from the second term in the above expression is marginal [12]-[13]. For relative ranking of the principal participating states in particular modes, the second term in the generic second order expression of participation factors can be ignored. Therefore, the participating factor p_{2ik} has been used to determine the ranking of the principal participating states in a particular inter-area mode as shown in TABLE II. TABLE II lists the top 5 normalized participation factors (NPFs) and corresponding states in each inter-area mode for all the controllers. It should be noted that all of the Lyapunov controllers - LYP1, LYP2, LYPF1 and LYPF2 exhibit high participation factors from rotor speed and rotor angles (electromechanical states). However, LYP1, LYP2 and LYPF1 also have significant participation factors from controller/non electromechanical states, with LYP2 having highest participation from a controller state. In other words, the three feedback linearization based Lyapunov controllers significantly modify the mode-shapes of interarea modes via high participation of electrical/controller states and large control effort. As any type of Lyapunov control or PSS control that we have studied in this paper is after all a type of excitation control (which controls the excitation voltage of the machine, which then influences the developed torque, which in turn influences the rotor angle), ideally excitation control shouldn't have a direct influence on the inter-area modes from controller/electrical states, and this is true for both PSS and LYPF2. But this is not true for LYP1, LYP2 and LYPF1, where we see direct influence from control/electrical states in the inter-area modes, and which also leads to reduction in their modal frequencies to values which are usually not observed for interarea modes (that is, frequencies less than 0.2 Hz) [16]. It should be noted here that the change in modal properties depend upon control parameters, total control effort, the feedback variables and state participation factors [28]. The overall damping of modal oscillations in the power system is decided not only by the frequencies of the dominant modes, but also by the damping ratios of those modes [17]. Thus, the reduction in frequencies of the inter-area modes in the case of LYP1, LYP2 and LYPF1 has no apparent adverse effect on control performance because this reduction is well compensated by a significant increase in damping ratios. Nevertheless, the associated modification of the inherent nature of the inter-area modes is not desirable as it can have an adverse effect on the stability of the system in the long run.

E. Total Control Cost

The total cost is a sum of the control effort and state deviations [25]. The control effort (CE) for each machine is measured as the square of deviation in control input, which is E_{fd}, from its steady state value. State deviation (SD) for each machine is measured as the sum of square of deviations in the seven states (δ, ω, E'_d, E'_q, ψ_{1d}, ψ_{2q}, E'_{dc}) from their respective nominal values. In this case study, a 1% step change in input mechanical torque was applied at $t = 10s$ as a disturbance to each machine in the system. The deviations were sampled at 100Hz and are accumulated for 15 seconds (from $t = 10s$ to $t = 25s$). A sample plot of control effort with different controllers for machine 1 is shown in Fig. 8. For a small disturbance, 15 seconds are adequate for the system to settle down to a new steady state. TABLE III lists the control effort (32) and state deviation (33) for each controller.

$$\mathrm{CE} = \sum_{i=1}^{p} \left[\sum_{k=\underline{k}}^{\bar{k}} \left(E_{fdi}^{k} - E_{fd0i}^{k}\right)^{\mathrm{T}} \left(E_{fdi}^{k} - E_{fd0i}^{k}\right) \right] \quad (32)$$

$$\mathrm{SD} = \sum_{i=1}^{p} \left[\sum_{k=\underline{k}}^{\bar{k}} \left(\boldsymbol{x}_i^k - \boldsymbol{x}_{0i}^k\right)^{\mathrm{T}} \left(\boldsymbol{x}_i^k - \boldsymbol{x}_{0i}^k\right) \right] \quad (33)$$

where, $\boldsymbol{x}_i^k = \left[\delta_i^k, \omega_i^k, E_{di}^{\prime\, k}, E_{qi}^{\prime\, k}, \psi_{1di}^k, \psi_{2qi}^k, E_{dci}^{\prime\, k}\right]$, and $\underline{k}$ and $\bar{k}$ are the sampling instants at the start and the end, respectively, of the accumulation of CE and SD.

It may be observed from the above table that all the nonlinear controllers have a higher control cost than the conventional PSS. This is because nonlinear controllers tend to respond vigorously in order to maintain stability when subjected to either small or large disturbances ([1], [2], [14], [26]). On the other hand, nonlinear controllers behave differently with respect to state deviations. LYP2 exhibits very low state deviations. LYPF2 with AVR leads to a moderate state deviation that is the closest to that of PSS and AVR. LYP1 and LYPF1 have similar basis exhibit the highest state deviations. The cumulative costs of control in the case of LYPF2 with AVR are much lesser than other nonlinear controllers but higher than traditional PSS (TABLE III). It is important to note that too high control costs (in the case of LYP1, LYP2 and LYPF1) may cause

the over-fluxing of generator transformer, which is not desirable.

It was found that such high state deviations result from rotor angle excursions. As LYP1 and LYPF1 do not include rotor angle in feedback, the controller has no control over rotor angle. Thus, any disturbance leads to new steady state rotor angles and the controllers are not able to restore them back to nominal values. This, in turn, significantly increases the accumulated rotor angle deviation over time compared to other controllers.

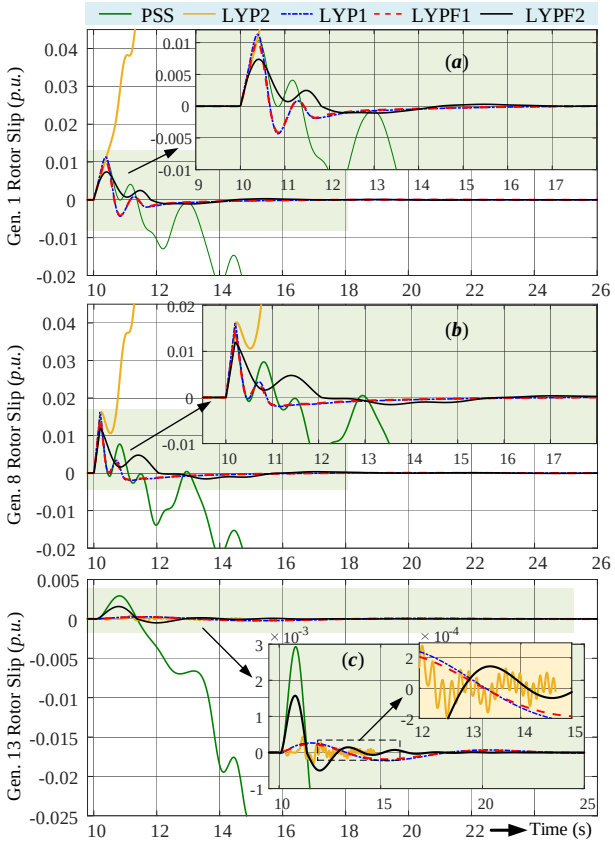

Fig. 9: Selected machine slips (system subjected to a 200ms fault).

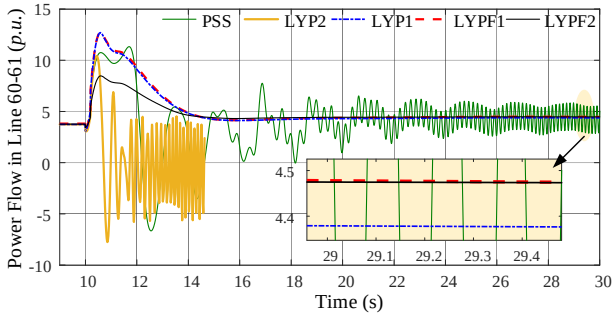

Fig. 10: Inter-area power flow (system subjected to a 200ms fault).

TABLE IV- TRANSIENT STABILITY INDICES

Controller	PSS	LYP1	LYP2	LYPF1	LYPF2
CCT (ms)	190	385	125	330	348
W_{tk}	1.531	0.112	4.576	0.121	0.117

TABLE V- CCT FOR DIFFERENT DISTURBANCE SCENARIOS

Faulted Line	↓ CCT (ms)	PSS	LYP1	LYP2	LYPF1	LYPF2
53-54		190	385	125	330	348
47-48		187	368.2	121	324.5	343
60-61		189	383.1	122.8	328	345.5

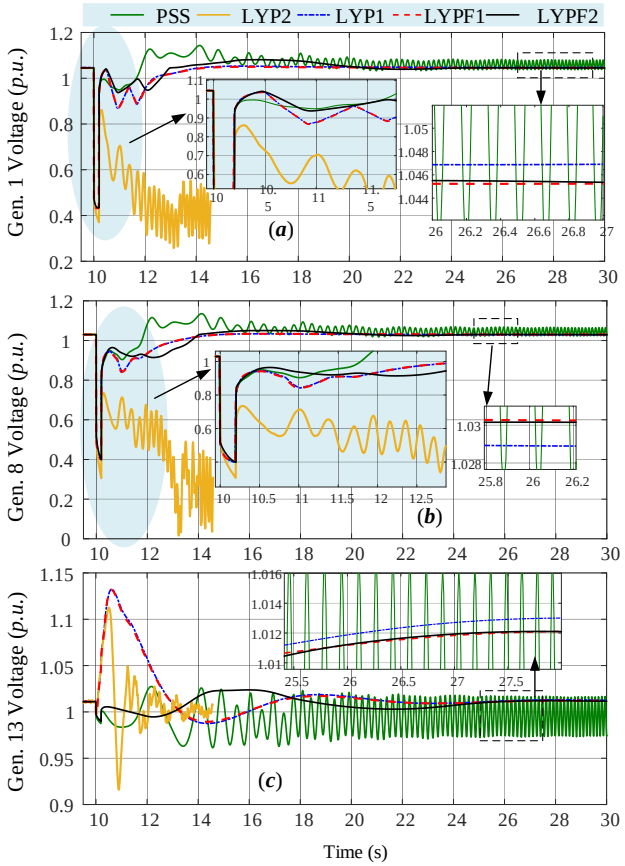

Fig. 11: Selected machine bus voltages (system subjected to a 200ms fault).

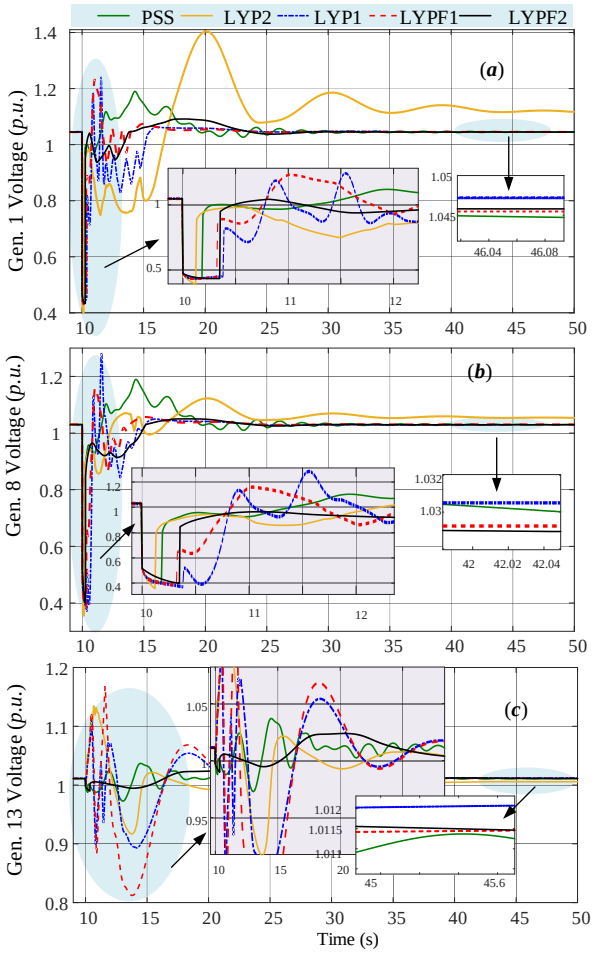

Fig. 12: Selected machine bus voltages showing post-fault dynamics.

F. Critical Clearing Time and Transient Stability Measure

Critical clearing time (CCT) refers to the longest time a fault can be tolerated by a system without losing stability. To find CCT, a three-phase symmetric fault was simulated by adding a large admittance to a bus node in system admittance matrix. The fault was simulated at bus 54 and cleared by opening circuit breakers on line 53-54. Faults of different time lengths were simulated until a CCT was found. System instability manifested itself as loss of synchronism, that is, non-zero rotor speed slips and irrevocable separation of machines into two mutually asynchronous groups. TABLE IV lists CCTs of each controller. Furthermore, slips and terminal voltages of machine 1, 8 and 13 and inter-area power flow (from NETS to NYPS through intertie 60-61) when subjected to a fault described above that lasts $200ms$ are shown in Fig. 9-Fig. 11. The three machines are chosen as they are electrically the closest and most remote from fault location, respectively (see Fig. 2).

For better understanding of the above CCT results an index W_{tk} (34) is defined as integrated variation of per-unit total energy exchanged between rotors of the generation units and the system has also been used for the transient stability evaluation (TSE) of the controllers. A lower value of TSE index indicates that the transient swings are smaller and TSE margins are better.

$$\mathrm{W}_{tk} = k_n \int_0^{\tau_{sim}} |d\mathrm{W}_t/dt| dt \tag{34}$$

where $\tau_{sim} = 30s$ is the observation period, W_t is the summation of per-unit energy exchanged and k_n is a normalization constant. W_t in (34) is calculated by using the rotor slip speeds (with center-of-inertia as frame of reference) of all the individual generation units.

$$\mathrm{W}_t = \sum_{i=1}^{p} \mathrm{M}_i S_i^2,\ S_i = \omega_i - \omega_{\mathrm{COI}} \tag{35}$$

where, $\omega_{\mathrm{COI}} = \left(\sum_{i=1}^{p} \mathrm{M}_i \omega_i\right) / \left(\sum_{i=1}^{p} \mathrm{M}_i\right)$. The corresponding values of W_{tk} are listed in TABLE IV. The disturbance in this case study lasts for $180ms$ (which is less than the least CCT amongst all the controllers other than LYP2). For further evaluation, faults were initiated near buses 47 and 60 of the test system (Fig. 2) and the faults were cleared by opening the breakers of the faulted lines. CCTs for these fault scenarios were obtained using the aforementioned procedure and the results have been presented in TABLE V. With LYP1, LYPF1 and LYPF2 controllers the CCT improves significantly compared to PSS and the results are consistent for any disturbance scenario.

G. Voltage regulation

It is vital for a power system to maintain terminal generator voltages at their nominal values in post-disturbance condition. In this case study, post-fault-clearing generator terminal voltages were studied for the critically cleared fault at bus 54. The post-fault terminal voltage of machine 1, 8 and 13 are shown (Fig. 12). Note that the controllers LYP1 and LYP2 settle down to a new steady state.

The controller is deemed effective if the post-disturbance voltage regulation of the generator buses is very small. The percentage voltage regulation of the i^{th} generator bus VR_i is given by (36). The voltage regulation indices; average (VR_{avg}) and maximum (VR_{max}) voltage regulations of the generator buses were used to quantify and study the effect of the studied controllers including proposed ones on the voltage regulation under various power disturbance scenarios. Three different disturbance scenarios were used to assess the impact of controllers on the voltage regulation. In the first disturbance scenario, a fault was simulated at bus 54 and cleared by opening circuit breakers on line 53-54. In the second disturbance scenario, a fault was simulated at bus 27 and cleared by opening circuit breakers on line 53-27. In the third disturbance scenario, the loads at bus 61 and bus 47 were increased by 10% and 7% respectively. The corresponding regulation indices are given in TABLE VI. As inferred from the tabulated results, controllers LYP1, LYPF1 and LYPF2 have good voltage regulation whereas with LYP2, the voltage regulation is relatively poor. Similar results were obtained by simulating multiple disturbance scenarios.

$$\mathrm{VR}_i = 100 \times (\mathrm{V}_{ti0} - \mathrm{V}_{ti\infty})/\mathrm{V}_{ti0} \tag{36}$$

where, V_{ti0} and $\mathrm{V}_{ti\infty}$ are respectively the pre-disturbance and post-disturbance bus voltages of the i^{th} generator.

Controllers LYP1, LYPF1 and LYPF2 have good voltage regulation (as illustrated in Fig. 12, TABLE VI), owing to the terminal voltage term in their feedback loops. However, LYP2 does not control the terminal voltage on its own. LYP2 requires switching to a voltage controller using a so-called 'membership function' in post-disturbance condition [7]. Fig. 11 also corroborates the above findings/inferences.

TABLE VI- VOLTAGE REGULATION; DIFFERENT DISTURBANCES

↓ Events		LYP1	LYP2	LYPF1	LYPF2
I	VR_{avg}	0.0269%	2.58%	0.0228%	0.0226%
	VR_{max}	0.0363%	5.26%	0.0261%	0.0258%
II	VR_{avg}	0.0277%	2.66%	0.0226%	0.0229%
	VR_{max}	0.0391%	5.47%	0.0258%	0.0262%
III	VR_{avg}	0.007%	1.94%	0.0047%	0.0052%
	VR_{max}	0.011%	3.73%	0.0049%	0.0057%

TABLE VII- ROOT MEAN SQUARE ERRORS FOR DSE

$\hat{x}_{13}$	**DSE (1%TVE)** RMSE ($p.u.$)	**DSE (1.5%TVE)** RMSE ($p.u.$)	**DSE (2%TVE)** RMSE ($p.u.$)
δ_{13}	6.54×10^{-3}	1.43×10^{-2}	2.31×10^{-2}
ω_{13}	4.08×10^{-4}	7.03×10^{-4}	1.11×10^{-3}
E'_{d13}	1.16×10^{-3}	2.56×10^{-3}	4.66×10^{-3}
E'_{q13}	1.71×10^{-3}	3.09×10^{-3}	5.27×10^{-3}
ψ_{1d13}	1.98×10^{-3}	7.10×10^{-3}	1.13×10^{-2}
ψ_{2q13}	2.33×10^{-3}	6.86×10^{-3}	1.06×10^{-2}

TABLE VIII- EFFECT OF DSE ON CONTROLLER PERFORMANCE

Controller →		LYP1	LYP2	LYPF1	LYPF2
0.5% TVE	Control effort	188.5	3×10^4	178.30	59.61
	State deviation	1115	1.358	992.31	57.74
	Total Cost	1303.5	3×10^4	1170.61	117.35
1% TVE	Control effort	188.7	3.1×10^4	178.32	59.62
	State deviation	1118	1.373	994.11	57.77
	Total Cost	1306.7	3.1×10^4	1172.43	117.39
2% TVE	Control effort	193.25	3.6×10^4	182.28	60.80
	State deviation	1129.4	1.557	1003.2	61.25
	Total Cost	1322.6	3.6×10^4	1185.48	122.05

TABLE IX-CONTROL INDICES: VARYING OPERATING CONDITIONS

↓ Operating Condition		LYP1	LYP2	LYPF1	LYPF2
I	Control effort	188.5	3×10^4	178.30	59.61
	State deviation	1115	1.358	992.31	57.74
	Total Cost	1303.5	3×10^4	1170.61	117.35
II	Control effort	190.5	3.1×10^4	180.75	60.01
	State deviation	1131.8	1.387	998.11	58.35
	Total Cost	1322.3	3.1×10^4	1178.86	118.36
III	Control effort	192.1	3.1×10^4	182.2	60.1
	State deviation	1142.1	1.399	1005.2	59.86
	Total Cost	1334.2	3.1×10^4	1187.4	119.96

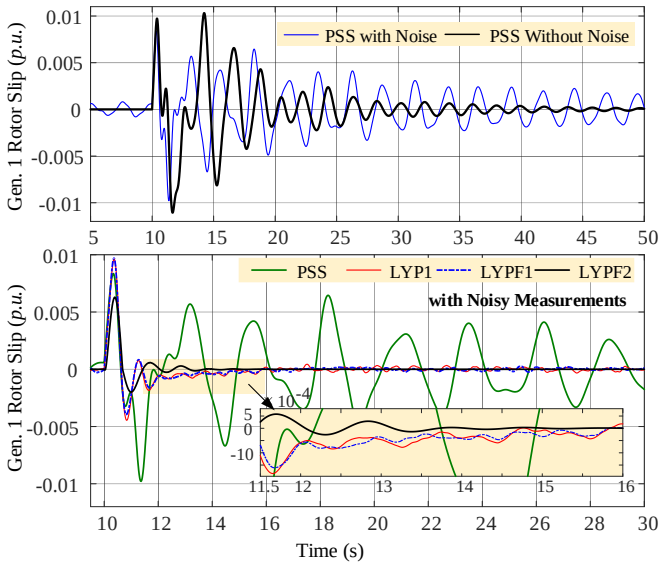

Fig. 13: Gen. 1. slip (system subjected to a 180ms fault).

H. Implementation and measurement noise

A general schematic of the implementation of these nonlinear controllers is shown in Fig. 3. Realization of these nonlinear controllers in practice (field) requires a dynamic state estimator (DSE) [27]-[31] to derive the unmeasurable states from the terminal measurements of the generation unit. A noisy measurement acts as an impediment in the realization of any control law particularly when derivative terms feature in it. As derivative terms feature in the control law of the LYP1 and LYPF1, the presence of the DSE for realization of these nonlinear controllers brings additional benefits as a noise filter. Assuming a 1% total vector error in the measurements as per IEEE standards [34]-[35], the performance of all these controllers and PSS was evaluated as illustrated in Fig. 13. Since the DSE was used as the input stage of these controllers their performance remains almost unchanged. The performance of the PSS, however, deteriorates in the case of a noisy measurements, probably due to the noise accentuation by the washout filter.

All the aforementioned test cases were simulated considering 0.1% total vector error (TVE) in the PMU measurements which is less than 1% TVE as recommended by IEEE standard C37.118.1-2011 for PMUs [34]. For comparison, results have also been obtained considering 0.5%, 1% and 2% TVEs in the PMU measurements. The performance of the controllers does not change even when TVE is as high as 1% TVE, as the DSE estimates are accurate for measurement noises less than or equal to 1% TVE. However, the control performance is affected by inaccurate estimates which happens when the noise/bad-data (TVE) in the acquired phasor measurements is 2%. With 2% TVE the estimated state trajectories are less accurate as shown in TABLE VII in which the corresponding root mean square errors in estimated states of the 13th generation unit of the test system are tabulated. In the case of LYP1, LYP2 and LYPF1, the cost indices increases slightly for TVEs greater than 1%. However, the effect in the case of LYPF2 is too marginal to make any substantial impact on the performance of the controller. The costs shown in TABLE VIII illustrates the impact of the impact of the less accurate estimates on the performance of the controllers. Due to presence of derivative terms in the control laws, the increase in the cost indices with LYP1, LYP2 and LYPF1 controllers is more than LYPF2 controller. Lastly, bad-data in the measurements can be detected and corrected using the bad-data detection algorithm [15]. That way the impact of the noise/bad-data can be alleviated to ensure that it does not affect the controller performance.

I. Robustness to Varying Operating Conditions

The Lyapunov control laws (1), (2), (11) and (25) get adapted to the varying power system conditions. Therefore, these control designs remain valid for any operating condition. For three operating conditions, a 1% step change in input mechanical torque was applied at $t = 10s$ as a disturbance to each machine in the system. The deviations were sampled at 100Hz and are accumulated for 15 seconds (from $t = 10s$ to $t = 25s$). The cost indices were used to assess the performance of Lyapunov control designs for three different operating cases. Case-I is the base case (same case discussed in section-VI. , sub-section E.). In case-II, the real-power load on bus 61 of the test system (Fig. 2) was increased by 50MW. In case-III, the real-power load on bus 47 of the test system was increased by 70MW. As observed from the tabulated data of control indices (TABLE IX), the controller performance does not change (or the change is quite marginal) upon change in the operating conditions. Therefore the performance of all these controllers does not change with change in operating conditions.

J. Computational Requirements and Feasibility

For nonlinear Lyapunov design, the complete power system simulation (along with the DSEs and the controllers at each generation unit of the test system) was performed in real-time (RT) simulation environment. A $100s$ simulation takes an average running time of $29.4s$, $32.8s$, $32.9s$, and $38.7s$ for the LYP1, LYP2, LYPF1 and LYPF2 respectively on a personal computer with $i7$-4970S-CPU, 2GHz Intel-processor and 8 GB RAM. Additionally floating-point operations per second (FLOPS) [36] were also computed to assess the feasibility of their real-time application. All these Lyapunov designs use less than hundred thousand FLOPS. Therefore, their computational requirements can be met by an ordinary DSP processor with processing speed in MHz. Moreover, all these controllers are decentralized, rely on local measurements and are therefore not affected by the scalability of the system/application. OP5600 Opal-RT multiprocessors were also used to execute the test case scenario in real-time Fig. 14. In this test case scenario, a

fault is simulated at bus 54 of the IEEE 68 bus test system for $200ms$ and the fault is cleared by opening circuit breakers on line 53-54. QNX platform based Opal-RT multiprocessor was used to emulate the power system and network dynamics and therefore worked as a real-time station and a Linux Redhat OP5600 core implemented the proposed **LYPF2** algorithm. The host command station with RT-lab (personal computer with $\boldsymbol{i7}$-4970S CPU, 2GHz processor and 8GB RAM), real-time station (RTS) and Redhat core2 (implementing LYPF2 scheme) interact between themselves through $\mathbf{100Mbit/}\boldsymbol{s}$ ethernet connection. Built-in DAC/ADC modules act as interface between the two Opal-RT cores and it was virtually impossible for the LYPF2 controller to distinguish between the emulated and the actual plant. Tektronix-MDO4054B-3 oscilloscope was used to capture the RT results (Fig. 14).

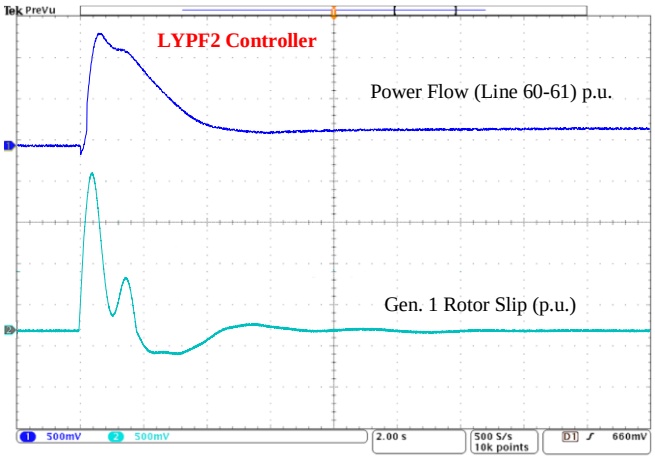

Fig. 14: Real-time results: LYPF2 performance in real-time (RT)

K. Potential for Field Application

The case studies presented in the paper establish the theoretical applicability of these Lyapunov based control methods. However, their dependencies must be considered for their field applicability. All these controllers are a direct application of dynamic state estimator (DSE), and therefore their practical realization also depends on how swiftly DSE is adopted by the industry. Since DSE is a fairly new technology, it requires reasonable time to be adopted by the power system industry. DSE has been widely researched in the field of power systems, and shows very promising potential for industry application. ABB Research Ltd. has filed a patent on "parallel computation of DSE" implying the adoption of DSE technology by the industry [37]. Similar patents on DSE technology were filed recently [38], [39]. The practical impediments and associated drawbacks of DSE have been studied /addressed in the recent power system literature [29], [40]. Therefore, with a high potential for DSE technology, the Lyapunov control for power systems discussed in the paper has a potential to be adopted for oscillatory control of future power systems.

L. Discussions

For the various case studies presented, the five questions that the research aims to answer may be revisited. Firstly, compatibility problem between the models used to design and test the controller does exist since even though LYP1 and LYP2 do not fail, they lead to a new system equilibrium, which may not be desired. Accordingly, one obvious advantage of controllers derived from sixth-order model (LYPF1 and LYPF2) over that derived from third-order model (LYP1 and LYP2) is that the controllers derived from sixth-order model are compatible with a detailed power system model, and hence, can be more realistically used for power system control.

Secondly, the nonlinear controllers have two advantages over PSS in the case study. All nonlinear controllers have a much higher damping ratio in inter-area modes than PSS and three nonlinear controllers (LYP1, LYPF1 and LYPF2) have much longer CCT for the faults simulated as compared to PSS. On comparing normal form-based control with Lyapunov based control, it can be observed that Lyapunov based controllers have better control performance as they have higher CCTs and better voltage regulation (please see [14] to compare the CCT and voltage regulation of normal form-based control with those presented in this paper).

Thirdly, the realization of all these Lyapunov controllers requires accurate estimation of machine states via dynamic state estimator. It has been established that detailed synchronous model is required to estimate these states accurately as estimates based on simplistic model are not accurate. Therefore, a detailed synchronous model is needed to perform DSE for realization of any Lyapunov controller.

Fourthly, without filtered measurements the performance (of all the controllers) is bound to deteriorate particularly in the case of controllers with derivative terms. However, the effect is alleviated by the DSE filter at the input of these nonlinear feedback controllers. It should be noted that amongst all the controllers, LYPF2 is least affected as it does not contain a derivative term in its feedback law. Moreover, the computation times for the Lyapunov controllers derived from sixth order model (LYPF1 and LYPF2) are marginally higher than their counterparts (LYP1 and LYP2) derived from third order model. However, all these controllers use less than hundred thousand FLOPS. Therefore, computation time is not an issue as their computational requirements can be met by a megahertz (MHz) processor.

Finally, all the three Lyapunov controllers based on feedback linearization and adaptive backstepping (LYP1, LYP2 and LYPF1) have drastic impact on the position of interarea modes because of which the frequencies of these modes are so much decreased that these modes are difficult to be classified as interarea modes. Moreover, the total costs of control for the three controllers are also very high (as can be seen in TABLE III). This means that all the three controllers increase the synchronizing torque by a large extent (as explained in Section VI. D.) which can cause over-fluxing issues in practice. The proposed LYPF2 controller, on the other hand, has modal frequencies similar to that of the linear PSS controller and its total costs of control are of the same order as PSS, and at the same time LYPF2 can provide much higher damping to interarea modes and its transient stability indices (like CCT and W_{tk} (TABLE IV)) are much better than PSS. Thus, the proposed nonlinear controller provides the best features of both linear

and nonlinear control and can be used safely without changing the inherent nature of a power system. This is an advantage which may prove to be critical for field implementation of Lyapunov control (and nonlinear control in general) in power systems. It should be noted that the adoption of the Lyapunov methodologies for oscillatory control in power systems depends on how swiftly DSE is adopted by the power system industry.

VII. Conclusion

In this paper, the control performance of various Lyapunov based nonlinear controllers was studied for the benchmark NETS-NYPS test system. It was found that nonlinear controllers derived from third-order machine models are not compatible with detailed power system models and, hence, nonlinear controllers should be derived from a detailed subtransient model of a machine. It was also found that nonlinear controllers can have an advantage in modal behavior, CCT, voltage regulation and robustness to noise (due to DSE) over a PSS. Also, Lyapunov based controllers show better performance as compared to normal form [14] based methods. The drawback of existing Lyapunov controllers has also been identified in terms of severe impact on interarea modes, very high costs of control and unrealistically high synchronizing torques. A new derivative free Lyapunov controller (LYPF2) has been proposed to address these drawbacks and serve as practical solution for field implementation of nonlinear control.

Appendix-A

IEEE 2.2 Model with Turbine Governor Dynamics [41]:

$$\Delta\dot{\delta}_i = \omega_i - \omega_s = \Delta\omega_i \tag{A1}$$

$$2H_i\Delta\dot{\omega}_i = \omega_s(T_{mi} - T_{ei}) - D_i\Delta\omega_i \tag{A2}$$

$$T'_{q0i}\dot{E}'_{di} = \left\{-E'_{di} - (x_{qi} - x'_{qi})\left[K_{q1i}I_{qi} + K_{q2i}\frac{\psi_{2qi} - E'_{di}}{x'_q - x_{li}}\right]\right\} \tag{A3}$$

$$T'_{d0i}\dot{E}'_{qi} = E_{fdi} - E'_{qi} + (x_{di} - x'_{di})\left[K_{d1i}I_{di} + K_{d2i}\frac{\psi_{1di} - E'_{qi}}{x'_{di} - x_{li}}\right] \tag{A4}$$

$$T''_{d0i}\dot{\psi}_{1di} = \left[E'_{qi} + (x'_{di} - x_{li})I_{di} - \psi_{1di}\right] \tag{A5}$$

$$T''_{q0i}\dot{\psi}_{2qi} = \left[E'_{di} + (x'_{qi} - x_{li})I_{qi} - \psi_{2qi}\right] \tag{A6}$$

$$T_{ci}\dot{E}'_{dci} = \left[(x''_{di} - x''_{qi})I_{qi} - E'_{dci}\right] \tag{A7}$$

$$P_{ei} = V_{di}I_{di} + V_{qi}I_{qi}, Q_{ei} = V_{di}I_{qi} - V_{qi}I_{di} \tag{A8}$$

where $V_{di} = -\mathrm{V}_{ti}\cos(\delta_i - \theta_i)$, $V_{qi} = \mathrm{V}_{ti}\sin(\delta_i - \theta_i)$ and

$$\begin{bmatrix} I_{di} \\ I_{qi} \end{bmatrix} = \begin{bmatrix} R_{ai} & x''_{qi} \\ x''_{di} & R_{ai} \end{bmatrix}^{-1} \begin{bmatrix} E'_{di}K_{q1i} - \psi_{2qi}K_{q2i} - V_{di} \\ E'_{qi}K_{d1i} - \psi_{1di}K_{d2i} - V_{qi} \end{bmatrix} \tag{A9}$$

However, R_{ai} usually is much smaller compared tox''_{qi} and x''_{di}, and the above equation gets simplified as follows.

$$I_{di} = \left(E'_{qi}K_{d1i} - \psi_{1di}K_{d2i} - V_{qi}\right)/x''_{di} \tag{A9.1}$$

$$I_{qi} = \left(E'_{di}K_{q1i} - \psi_{2qi}K_{q2i} - V_{di}\right)/x''_{qi} \tag{A9.2}$$

With (A8), (A9.1) and (A9.2), torque T_{ei} can be calculated as:

$$T_{ei} = \omega_i^{-1}P_{ei} = E'_{qi}I_{qi}K_{d1i} + E'_{di}I_{di}K_{q1i} + \left(x''_{di} - x''_{qi}\right)I_{qi}I_{di} - \psi_{2qi}I_{qi}K_{q2i} + \psi_{1di}I_{di}K_{d2i} \tag{A10}$$

The third-order machine model is a simplified model where subtransient dynamics are neglected by removing the damper windings. Equations (A1)-(A2) still hold for this model. The remaining equations for the model are as follows [19].

$$T'_{d0i}\dot{E}'_{qi} = E_{fdi} - E_{qi} \tag{A11}$$

$$E_{qi} = E'_{qi} + (x_{di} - x'_{di})I_{di} \tag{A12}$$

$$V_{di} = x'_{qi}I_{qi}, V_{qi} = E'_{qi} - x'_{di}I_{di} \tag{A13}$$

$$P_{ei} = E'_{qi}I_{qi}, \quad Q_{ei} = x_{di}^{-1}\mathrm{V}_{ti}\left(E_{qi} - \mathrm{V}_{ti}\right) \tag{A14}$$

Furthermore, automatic voltage regulators (AVRs) through excitation control regulate the generator terminal voltage at its nominal value. In this paper, it is assumed that all AVRs are assumed to be the standard static exciters (ST1A), with equations given as follows [15].

$$T_{ri}\dot{V}_{ri} = \mathrm{V}_{ti} - V_{ri} \tag{A15}$$

$$E_{fdi} = K_{Ai}\left(V_{refi} + V_{ssi} - V_{ri}\right) \tag{A16}$$

Standard TGOV1 model (17)-(18) represents the turbine-governor dynamics [20].

$$T_{\mathrm{CH}i}\dot{T}_{mi} = -T_{mi} + P_{\mathrm{SV}i} \tag{A17}$$

$$T_{\mathrm{SV}i}\dot{P}_{\mathrm{SV}i} = -P_{\mathrm{SV}i} + P_{\mathrm{C}i} - R_{\mathrm{D}i}^{-1}\Delta\omega_i/\omega_s \tag{A18}$$

The network interface, network equations and loads are represented by (19)-(22) equations [15].

$$I_{\mathrm{Q}i} + jI_{\mathrm{D}i} = \left(I_{qi} + jI_{di}\right)e^{j\delta_i} \tag{A19}$$

$$V_{gi} = V_{\mathrm{Q}i} + jV_{\mathrm{D}i} = \left(V_{qi} + jV_{di}\right)e^{j\delta_i} \tag{A20}$$

$$I_{gi} = I_{\mathrm{Q}i} + jI_{\mathrm{D}i} + (R_{ai} + jx''_d)^{-1}V_{gi} \tag{A21}$$

$$\mathbf{V} = \mathbf{Z_{AUG}I}\ ,\ \mathbf{Z_{AUG}} = \mathbf{Y_{AUG}^{-1}} \tag{A22}$$

where, $\mathbf{Y_{AUG}} = \mathbf{Y_G} + \mathbf{Y_N} + \mathbf{Y_L}$, $\mathbf{Y_G} = diag(\mathrm{Y_{G1}}, \mathrm{Y_{G2}}, \dots, \mathrm{Y_{GN}})$, $\mathrm{Y_{G}}j = (R_{ai} + jx''_d)^{-1}$ when i^{th} generator is connected to j^{th} network node, otherwise $\mathrm{Y_{G}}j = 0$. $\mathbf{Y_N}$ is the network shunt admittance whereas $\mathbf{Y_L}$ is load admittance matrix [15],[16].

Appendix-B

Tuning of gain vector γ

Arbitrary choice of controller gain may not produce the desired results. Therefore, the gain vector γ is tuned using a meticulously justified gradient based tuning method (detailed in the chapter 7 of [23]) given by (B.1) below.

$$\dot{\gamma} = -\alpha_1\frac{\varrho}{(\varrho^{\mathrm{T}}\varrho + \alpha_2)^2}[\varrho^{\mathrm{T}}\gamma + \mathrm{Q}(\tilde{\boldsymbol{x}}_i) + (\tilde{\boldsymbol{\mu}}'_i)^T\mathrm{R}(\tilde{\boldsymbol{\mu}}'_i)] \tag{B.1}$$

where, $\varrho = \left[\partial\left(\mathrm{M}(\tilde{\boldsymbol{x}}_i)\right)/\partial\tilde{\boldsymbol{x}}_i\right][\boldsymbol{f}(\tilde{\boldsymbol{x}}_i) + \boldsymbol{g}(\tilde{\boldsymbol{x}}_i)\tilde{\boldsymbol{\mu}}'_i]$, $\alpha_1 = 7.6$, $\alpha_2 = 1$, $\mathrm{Q}(\tilde{\boldsymbol{x}}_i) = \tilde{\boldsymbol{x}}_i^{\mathrm{T}}\boldsymbol{I}_{n_x}\tilde{\boldsymbol{x}}_i$, $\mathrm{R} = \boldsymbol{I}_{n_\mu}$. $\boldsymbol{I}_{n_x}$ and $\boldsymbol{I}_{n_\mu}$ are the identity matrices of orders n_x and n_μ respectively.

E_{dci} dynamics is absent in 68 bus NETS-NYPS power system (Fig. 2) as all the generation units are turbo-generators (i.e., $x''_d = x''_q$). Therefore, the state vector dimension reduces to 7. For 9th generation unit the value of the gain vector γ in steady state is given below:

$$\begin{aligned}\gamma = [&-0.17 \quad 0.01 \quad 0.14 \quad -0.45 \quad 0.19 \quad 0.13 \quad 0 \quad \cdots\\ &0 \quad 0 \quad -0.01 \quad -0.02 \quad 0 \quad 0 \quad -0.095 \quad \cdots\\ &0.04 \quad -0.16 \quad -0.11 \quad 0 \quad 1.18 \quad 0.43 \quad -0.12 \quad \cdots\\ &0 \quad -0.17 \quad 0.13 \quad 0 \quad -0.09 \quad 0.01 \quad 0]^{\mathrm{T}}\end{aligned}$$

Power System Stabilizer Equations [15], [33], [28]-[40]

$$T_{wi}\dot{p}_{s1i} = p'_{s1i}, \qquad p'_{s1i} = K_{Si}\Delta\omega_i - p_{s1i} \tag{B. 2}$$

$$T_{12i}\dot{p}_{s2i} = p'_{s2i}, \qquad p'_{s2i} = p'_{s1i} - p_{s2i} \tag{B. 3}$$

$$T_{22i}\dot{p}_{s3i} = p'_{s3i},$$

$$p'_{s3} = p'_{s1} + (T_{11i} - T_{12i})\,p'_{s2}/T_{12i} - p_{s3} \tag{B. 4}$$

$$\mathrm{V}_{ssi} = p'_{s1\mathrm{i}} + (T_{11i} - T_{12i})\,p'_{s2}/T_{12i} + (T_{21i} - T_{22i})\,p'_{s3}/T_{22i} \tag{B. 5}$$

$$E_{fdi} = K_{Ai}(V_{refi} + V_{ssi} - V_{ri}) \tag{B. 6}$$

REFERENCES

[1] Q. Lu, Y. Z. Sun, Z. Xu and T. Mochizuki, "Decentralized nonlinear optimal excitation control," *IEEE Trans. Power Syst.*, vol. 11, no. 4, pp. 1957-1962, Nov. 1996.

[2] M. A. Mahmud, H. R. Pota, M. Aldeen and M. J. Hossain, "Partial Feedback Linearizing Excitation Controller for Multimachine Power Systems to Improve Transient Stability," *IEEE Trans. Power Syst.*, vol. 29, no. 2, p. 561–571, Mar. 2014.

[3] W. Yao, L. Jiang, J. Fang, J. Wen and S. Cheng, "Decentralized nonlinear optimal predictive excitation control for multi-machine power systems," *Int. J. of Elec. Power & Energy Syst.*, vol. 55, pp. 620-627, 2014.

[4] Y. Guo, D. J. Hill and Y. Wang, "Global transient stability and voltage regulation for power systems," *IEEE Trans. Power Syst.*, vol. 16, no. 4, pp. 678-688, Nov. 2001.

[5] J. W. Chapman, M. D. Ilic, C. A. King, L. Eng and H. Kaufman, "Stabilizing a multimachine power system via decentralized feedback linearizing excitation control," *IEEE Trans. Power Syst.*, vol. 8, no. 3, pp. 830-839, Aug. 1993.

[6] H. Liu, Z. Hu and Y. Song, "Lyapunov-Based Decentralized Excitation Control for Global Asymptotic Stability and Voltage Regulation of Multi-Machine Power Systems," *IEEE Trans. Power Syst.*, vol. 27, no. 4, pp. 2262-2270, Nov. 2012.

[7] R. Yan, Z. Y. Dong, T. K. Saha and R. Majumder, "A power system nonlinear adaptive decentralized controller design," *Automatica*, vol. 46, no. 2, pp. 330-336, Feb. 2010.

[8] Y. Wang, D. Cheng, C. Li and Y. Ge, "Dissipative Hamiltonian realization and energy-based L2-disturbance attenuation control of multimachine power systems," *IEEE Trans. Automatic Control*, vol. 48, no. 8, pp. 1428-1433, Aug. 2003.

[9] Q. Lu, S. Mei, W. Hu, F. Wu, Y. Ni and T. Shen, "Nonlinear decentralized disturbance attenuation excitation control via new recursive design for multimachine power systems," *IEEE Trans. Power Syst.*, vol. 16, no. 4, pp. 729-736, Nov. 2001.

[10] Y. Guo, D. J. Hill and Y. Wang, "Nonlinear decentralized control of large-scale power systems," *Automatica*, vol. 36, no. 9, pp. 1275-1289, Sep. 2000.

[11] *IEEE Guide for Synchronous Generator modelling Practices and Applications in Power System Stability Analyses*, IEEE Std 1110-2002 (Revision of IEEE Std 1110-1991), 2003.

[12] J. J. Sanchez-Gasca, et. al., "Inclusion of higher order terms for small-signal (modal) analysis: committee report-task force on assessing the need to include higher order terms for small-signal (modal) analysis," *IEEE Trans. Power Syst.*, vol. 20, no. 4, pp. 1886-1904, Nov. 2005.

[13] M. Netto, Y. Susuki and L. Mili, "Data-Driven Participation Factors for Nonlinear Systems Based on Koopman Mode Decomposition," *IEEE Control Syst. Letters*, vol. 3, no. 1, pp. 198-203, Jan. 2019.

[14] A. K. Singh and B. C. Pal, "Decentralized Nonlinear Control for Power Systems using Normal Forms and Detailed Models," *IEEE Trans. Power Syst*., vol. 33, no. 2, pp. 1160-1172, March 2018.

[15] A. K. Singh and B. C. Pal, *Dynamic Estimation and Control of Power Systems*. London, U.K.: Academic Press, 2019.

[16] K. R. Padiyar, *Power System Dynamics*: *Stability and Control*, Tunbridge Wells: Anshan Limited, 2004.

[17] P. Kundur, *Power System Stability and Control*, New York: McGraw-Hill, 1994.

[18] B. Pal and B. Chaudhuri, *Robust Control in Power Systems*, New York: Springer, 2005.

[19] Z. Li, Y. Yang and X. Bao, "Simulation and Analysis of the Third-order Model of Synchronous Generator based on MFC," in *IEEE International Conference on Mechatronics and Automation, ICMA* , Changchun, China, 2009.

[20] Peter W Sauer and M. A Pai. *Power system dynamics and stability*. English. Champaign, IL.: Stipes Publishing L.L.C., 2006.

[21] Mathworks, "Output time derivative of input," [Online]. Available: https://uk.mathworks.com/help/simulink/slref/derivative.html.

[22] A. Isidori, *Nonlinear Control Systems*, London, U.K: Springer, 1995.

[23] D. Vrabie, K. Vamvoudakis and F.L. Lewis, *Optimal Adaptive Control and Differential Games by Reinforcement Learning Principles*, London, U.K.: IET Press, 2012.

[24] M. Gopal, *Digital Control and State Variable Methods*, Tata McGraw-Hill Education, 2003.

[25] A. K. Singh and B. C. Pal, "Decentralized Control of Oscillatory Dynamics in Power Systems Using an Extended LQR," *IEEE Trans. Power Syst*., vol. 31, no. 3, pp. 1715-1728, May 2016.

[26] A. S. Mir, S. Bhasin and N. Senroy, "Decentralized Nonlinear Adaptive Optimal Control Scheme for Enhancement of Power System Stability," *IEEE Trans. Power Syst*., vol. 35, no. 2, March 2020.

[27] H. K. Khalil, *Nonlinear Systems*, 3rd ed. Upper Saddle River, NJ: Prentice-Hall, 2000.

[28] R. Jabr, B. Pal and N. Martins, "A sequential conic programming approach for the coordinated and robust design of power system stabilizers," *IEEE Trans. Power Syst*., vol. 25, no. 3, pp. 1627-1637, Aug. 2010.

[29] Y. Liu et al., "Dynamic State Estimation for Power System Control and Protection," *IEEE Trans. Power Syst*.,, vol. 36, no. 6, pp. 5909-5921, Nov. 2021.

[30] J. Zhao et al., "Power System Dynamic State Estimation: Motivations, Definitions, Methodologies, and Future Work," *IEEE Trans. Power Syst*., vol. 34, no. 4, pp. 3188-3198, July 2019.

[31] A. K. Singh and B. C. Pal, "Decentralized Dynamic State Estimation in Power Systems Using Unscented Transformation," *IEEE Trans. Power Syst*., vol. 29, no. 2, pp. 794-804, March 2014.

[32] S. Julier, et. al.,, "A new method for the nonlinear transformation of means and covariances in filters and estimators," *IEEE Trans. Autom. Control*, vol. 45, no. 3, pp. 477–482, Mar. 2000.

[33] A. A. Sallam, O. P. Malik, *Power System Stability: Modelling, Analysis and Control*, Power and Energy Series, IET Press, 2015.

[34] *IEEE Standard for Synchrophasor Measurements for Power Systems*, IEEE Std. C37.118.1–2011, Dec. 2011.

[35] A. G. Phadke and J. S. Thorp, *Synchronized Phasor Measurements and Their Applications*. New York, NY, USA: Springer, 2008.

[36] H. Qian (2020), Counting the floating point operations (FLOPS) https://www.mathworks.com/matlabcentral/fileexchange/50608counting-the-floating-point-operations-flops. Accessed: Dec, 18, 2020.

[37] E. Scholtz, V. Donde, and J. Tournier, "Parallel computation of dynamic state estimation for power system," U.S. Patent Application 13/832670, Mar. 15, 2013.

[38] A. Singh, and B. Pal, "Dynamic state estimation of an operational state of a generator in a power system" U.S. Patent Application 2020/0132772A1, Apr. 30, 2020

[39] R. Dai, G. Liu, C. Yuan, P. Wei, Y. Zhu, Y. Lu, Z. Liao and Z. Wang, "Systems and methods for hybrid dynamic state estimation" U.S. Patent Application 11119462B2, Sept. 14, 2021

[40] J. Zhao *et al*., "Power system dynamic state and parameter estimation-transition to power electronics-dominated clean energy systems," *IEEE PES Task Force on Power System Dynamic State and Parameter Estimation*, Piscataway, NJ, USA, Tech. Rep. PES-TR88, Jul. 2021.

[41] C. Canizares *et al*., "Benchmark systems for small-signal stability analysis and control," *IEEE PES Task Force on Benchmark Systems for Stability Controls*, Piscataway, NJ, USA, Tech. Rep. PES-TR18, Aug. 2015.

Abdul Saleem Mir (S'19–M'22) received his B. Tech. degree (Hons.) in Electrical Engineering from National Institute of Technology, Srinagar, J&K, and Ph.D. degree in Electrical Engineering from Indian Institute of Technology Delhi, India, in 2014 and 2020 respectively. He is currently an Assistant Professor in the Department of Electrical Engineering, Indian Institute of Technology Roorkee, India. From October 2020 to December 2021, he was a Research Fellow at the University of Southampton with Imperial College London as collaboration Institute. He is a member of IEEE PES Task Force on Dynamic State and Parameter Estimation and IEEE PES Task Force on Standard Test Cases for Power System State Estimation. He was awarded IEEE PES Working Group Member Recognition Award in 2022 for his contributions to IEEE PES TF on Dynamic State and Parameter Estimation. His research interests include dynamic state estimation and control, power system dynamics and modeling/control of renewable energy systems.

Abhinav Kumar Singh (S'12–M'15) received his B. Tech. degree in Electrical Engg. from Indian Institute of Technology Delhi, India, and Ph.D. degree in EE from Imperial College London, U.K. in 2010 and 2015 respectively. He is a Lecturer at the School of Electronics and Computer Science, University of Southampton. Previously, he was a Lecturer at the University of Lincoln from Aug 2017 to Mar 2019, and a Research Associate at Imperial College London from Jan 2015 to July 2017. He won IEEE PES Working Group Recognition Award in 2016 for his contributions to IEEE PES task force on benchmark systems. He was awarded IEEE PES Working Group Recognition Awards in 2016 and 2022 for his contributions to two IEEE PES Task Forces. He is a member of IEEE PES Task Force on Dynamic State and Parameter Estimation and IEEE PES Task Force on Standard Test Cases for Power System State Estimation. He currently serves as an Editor of IEEE Transactions on Power Systems. His research interests include real-time estimation and control of future energy networks.

Bikash C. Pal (M'00-SM'02-F'13) received B.E.E. degree (with honors) from Jadavpur University, Calcutta, India, M.E. degree from the Indian Institute of Science, Bangalore, India, and Ph.D. degree from Imperial College London, London, U.K., in 1990, 1992, and 1999, respectively, all in electrical engineering. Currently, he is a Professor in the Department of Electrical and Electronic Engineering, Imperial College London. His research interests include renewable energy modelling and control, state estimation, and power system dynamics. He is Vice President Publications, IEEE Power & Energy Society. He was Editor-in-Chief of IEEE Transactions on Sustainable Energy (2012-2017) and Editor-in-Chief of IET Generation, Transmission and Distribution (2005-2012) and is a Fellow of IEEE for his contribution to power system.

Nilanjan Senroy (S'01–M'06-SM'18) received the B. Tech. degree from the National Institute of Technology, Jamshedpur, India, and the M.S. and Ph.D. degrees from Arizona State University, Tempe, AZ, USA. He also has postdoctoral experience at the Center for Advanced Power Systems, Florida State University, Tallahassee, FL, USA. He is currently Power Grid Chair Professor in the Department of Electrical Engineering, Indian Institute of Technology Delhi, India. He currently serves as an Editor of IEEE Transactions on Power Systems and IEEE PES Letters. His research interests include power system stability and control, dynamics, modeling and simulation of wind energy conversion systems and signal processing techniques in power systems.

Junjie Tu was a masters student of electrical engineering at Imperial College London, London, U.K. His research interests include power system dynamics and control.